Chapter VIII – Remote Sensing

I - Introduction to remote sensing

See slides by Séverine Alvain

II - Principles of "ocean colour" remote sensing from space

[adapted from "Apports de la télédétection spatiale de la 'couleur' de l'océan à l'océanographie", *Océanis*, 1998, by David Antoine]

"We must first understand that by remote sensing of "ocean colour" we are trying to quantify a geophysical variable, namely the concentration of chlorophyll. One can imagine the difficulty of this operation, which begins with measuring the radiance outside the atmosphere and is thus much more challenging than the qualitative use of satellite measurements (generally the only one known to the general public from weather forecasts or for military purposes). Ocean colour measurements are generally limited to simple signal processing for pattern recognition or classification of various objects. In this chapter, the whole process is described in three stages, each posing different challenges: (i) the measurement of radiance outside the atmosphere, (ii) the atmospheric correction of this radiance, and (iii) calculating the concentration of chlorophyll based on this corrected signal.

Measuring radiance outside the atmosphere

An instrument dedicated to the remote sensing of ocean colour measures a certain amount of radiative energy and converts this into an electric current strength that is proportional to the amount of radiative energy received. This analogue signal must then be digitized, treated (basic radiometric corrections: an initial calibration, applying gains, etc.), stored for later analyses, and sent to the satellite receiving stations on the ground. The amount of radiative energy measured by the instrument depends on the part of the electromagnetic spectrum and on the **instantaneous field of view** (**Ifov**), which corresponds to the basic unit at which observations are available (pixel). The solid angle of such a pixel determines the size of the ocean surface that it corresponds to. One of the difficulties when constructing these instruments lies in establishing a sufficiently high signal/noise ratio* considering that the observed signal is typically very weak. Since electromagnetic radiation is recorded in small solid angles from given directions, it is a measure of radiance, referred to as total radiance, since its intensity in a given direction is determined by the optical properties of the ocean, by those at the air/sea interface, and by the optical properties of the atmosphere (including clouds if present). This radiance therefore contains information about the entire ocean-atmosphere system. As it is the ocean that interests us, we must first correct this signal for the effects of the atmosphere.

[* for more details; see the site by Mobley: https://www.oceanopticsbook.info/view/remote-sensing/level-2/counting-photons]

The atmospheric correction

In order to analyse the light backscattered by the ocean, it is necessary to extract from the total radiances (Lt or Lsat) the part that comes from the ocean, usually termed "water-leaving radiance" (Lw). All the necessary operations are usually grouped together under the term "atmospheric corrections". They consist of the elimination of the radiances due to scattering

by atmospheric molecules (Lr, Raleigh scattering) and aerosols (La and Lra in case of multiple scattering) and of radiances that never entered the ocean but were reflected at the ocean surface (Lg from "solar glint" and Lwc from "white caps"). While the subject is complex, we will only give a quick overview of some of the existing techniques. They are generally based on a decomposition of the signal into different contributions:

$$Lt = Lr + La + Lra + tLg + tLwc + tLw$$

The major contributions to the measured signal come from scattering by air molecules and aerosols (Lr + La + Lra often referred to as L*path*).

We deliberately omit absorption phenomena here for two reasons. First of all, we can assume that the sensors measure radiances that lie outside the earth's main atmospheric absorption bands; then, if any significant absorption should occur they will not "generate" any signal but, on the contrary, eliminate a certain number of photons of very specific wavelengths. The difficulty, in the event of absorption, then consists in correcting the measured signal in order to obtain a value in the absence of such absorptions. This neglects any linkages that exist between absorption and scattering. If scattering is important (multiple scattering), it can increase absorption as it increases the path lengths travelled by photons.

For a given scattering angle, the measured radiance is a function of the amount of "scattering material" and of the scattering indicatrix of this material. It is relatively easy to estimate the part of the signal that is due to scattering by molecules as the atmospheric pressure (and therefore the quantity of molecules in the atmospheric "column") is known, as well as the scattering indicatrix of those molecules. The contribution by molecular scattering can thus be calculated without difficulty, possibly taking into account the effect of polarization and also considering the state of the air/sea interface which affects the amount of reflected radiance (Gordon et al. , 1988; Gordon & Wang , 1992a, b + Hydrolight).

Estimating the contribution due to scattering by aerosols is more difficult, since neither their concentration nor their scattering indicatrix are known when attempting he atmospheric correction (aerosols are typically very diverse and also heterogeneously distributed in the atmosphere). Determining these two unknowns requires at least two equations, which means in practice that information must be obtained at two wavelengths at least. Most of the techniques currently in use are based on observations of the ocean-atmosphere system at two near-infrared wavebands in which the ocean signal is zero (at least for Case 1 waters). This is due to the very strong absorption of light in water and to the weak scattering capacities of the various suspended materials (with the exception of air bubbles). Once corrected for the effect of molecular scattering, the remaining signal is entirely due to aerosols."

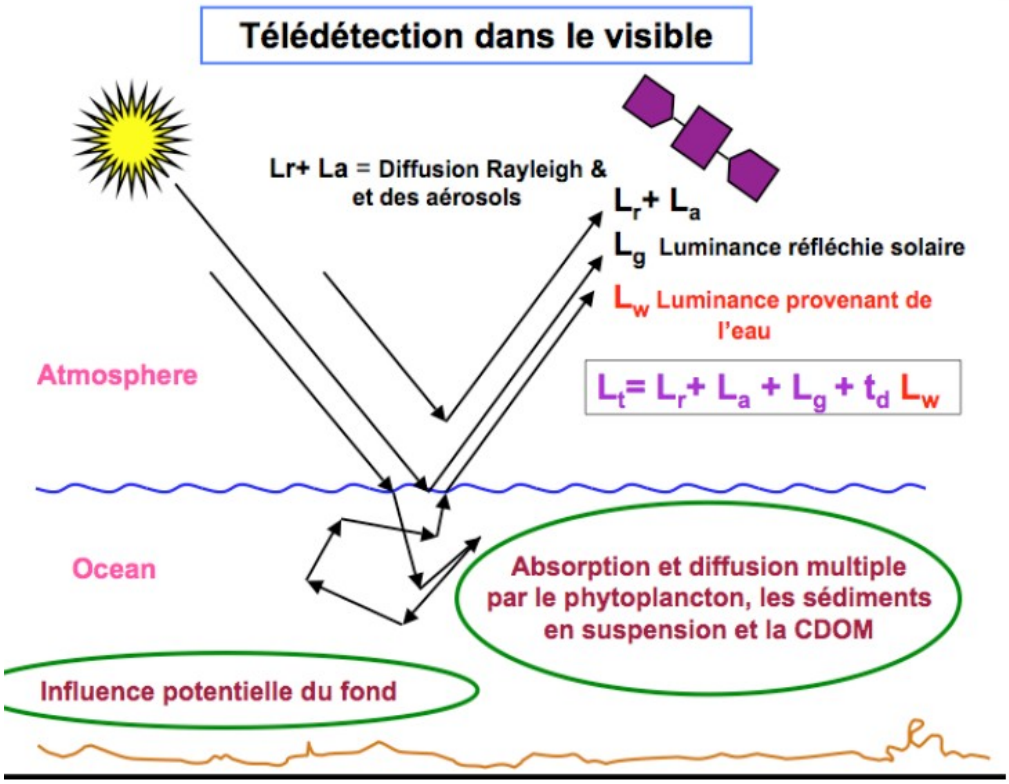

(courtesy M. Mohan, Space Applications Center, Ahmedabad; beware of an error: a transmission coefficient must be added before Lg)

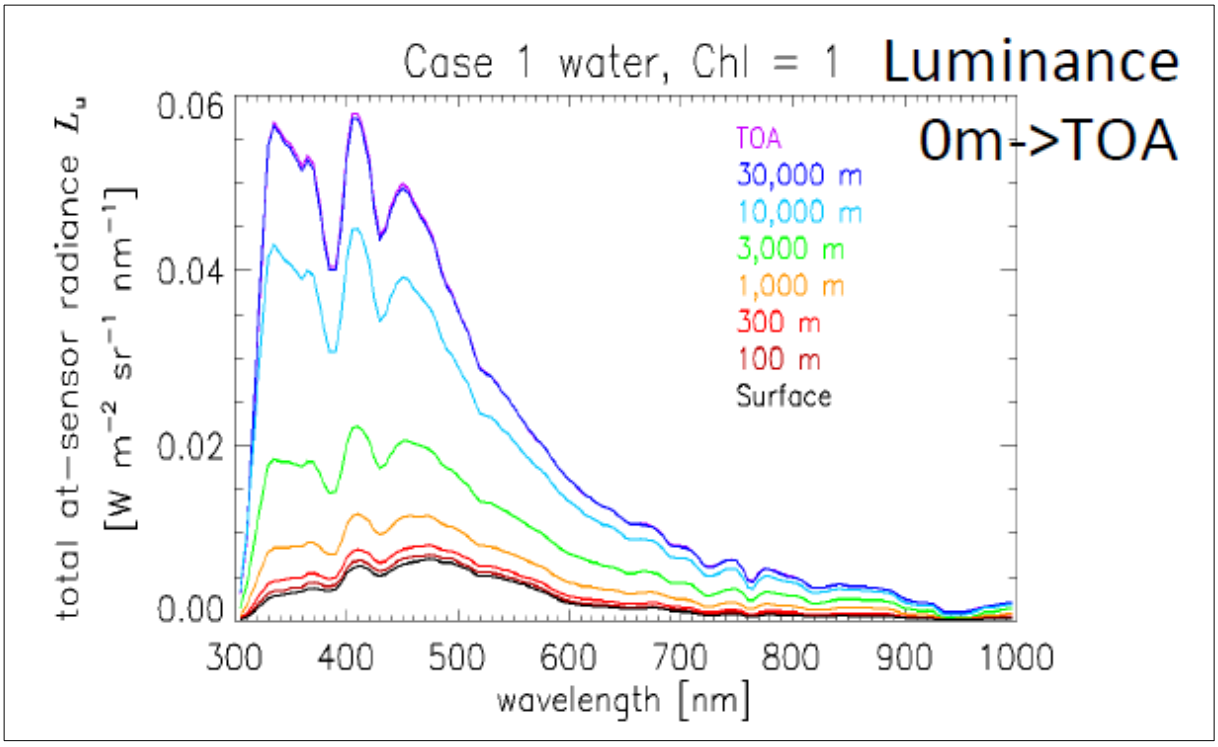

(after David Antoine excerpt from "Apports de la télédétection spatiale de la 'couleur' de l'océan à l'océanographie", *Océanis*, 1998)

From the intensity of this signal and its spectral dependence between the two wavelengths considered, we obtain sufficient information about the aerosols present to be able to extrapolate their contribution to visible wavelengths and thus perform the atmospheric cprrection (see, for example: Gordon, 1978; Bricaud & Morel, 1987; André & Morel, 1991; Gordon & Wang, 1994; Fraser et al., 1997; Gordon, 1997; Antoine & Morel, 1998, 1999)."

The third step consists of solving the **inverse problem of the water-leaving radiance** (the part concerning IOPs has already been summarised in Chapter 5). Additional details are provided here about the terminology used in scientific articles.

Definition of ρ

Most remote sensing algorithms us the remote sensing reflectance (unit: sr^{-1}) Rrs = Lw/Ed or an equivalent non-dimensional reflectance ρ=π Lw/Ed (if Lw was directionally isotropic, Rrs = 1/π, thus ρ is the ratio between the actual and ideal isotropic remote sensing reflectances). Using an apparent optical property like Rrs or ρ minimises any environmental effects, such as the solar angle, on the spectrum.
Note that ρ is dimensionless.

Normalisation of Lw

The normalisation can be achieved as follows. The first step consists of accounting for the effects of the solar zenith angle and the atmospheric attenuation on Lw($L_w(\theta_s, \theta_v, \phi)$ (e.g., Gordon and Clark (1981), p. 10,910; Gordon and Wang (1994b) using the equation:

$$L_w(\theta_v, \phi)_N = \frac{L_w(\theta_s, \theta_v, \phi)}{\cos\theta_s t(\theta_s)}$$

where $t(\theta_s)$ is the diffuse atmospheric transmittance for the irradiance in the direction of the sun for the given atmospheric conditions. Recent publications often include a correction factor to correct Lw for annual variations in the earth-sun distance:

$$L_w(\theta_v, \phi)_N = \left(\frac{R}{R_o}\right)^2 \frac{L_w(\theta_s, \theta_v, \phi)}{\cos\theta_s t(\theta_s)}$$

Here, R is the earth-sun distance at the time of measurement and Ro is the mean earth-sun distance. The factor $\left(\frac{R}{R_o}\right)^2$ thus corrects Lw with respect to the mean earth-sun distance. (The solar irradiance at the top of the atmosphere varies by about 8% throughout the year due to the ellipticity of the earth's orbit.)

$L_w(\theta_v, \phi)_N$ is called the **normalised water-leaving radiance**. It is the water-leaving radiance for the case of mean earth-sun distance, the sun at the zenith, and without any atmospheric attenuation. Note that although the factors $\left(\frac{R}{R_o}\right)^2$, $\cos\theta_s$, and $t(\theta_s)$ largely remove the respective effects of a varying earth-sun distance, solar zenith angle, and atmospheric attenuation on $L_w(\theta_v, \phi)_N$; $L_w(\theta_v, \phi)_N$ still depends on the angle of observation (solid angle) and on the angular distribution of sky diffuse radiance at the time of

the observation.

By multiplying $L_w(\theta_v,\phi)_N$ with a factor π/Fo where π has units of steradian and Fo is the irradiance arriving at the top of the atmosphere when the earth is at its average distance from the sun, we obtain the dimensionless normalised water-leaving reflectance (Gordon et Wang (1994b), p. 7756):

$$\rho_w(\theta_v,\phi)_N=\frac{\pi}{F_o}L_w(\theta_v,\phi)_N=\pi\frac{\left(\frac{R}{R_o}\right)^2 L_w(\theta_s,\theta_v,\phi)}{F_o\cos\theta_s t(\theta_s)} \quad \text{and} \quad \rho_w(\theta_v,\phi)_N=\pi R_{rs}(\theta_v,\phi)$$

We note that $\rho_w(\theta_v,\phi)_N$ is dimensionless.

III- Processing Levels

Data can be viewed and retrieved in a variety of formats and processing levels. There are five general levels of processing ranging from raw (unprocessed) output to modelled output.

Level 0 raw unprocessed data, typically not provided to users

Level 1 measured data with no or only minimal processing (e.g., radiometric measurements such as radiances in W/nm/sr)

Level 2 derived geophysical variables (e.g., geostrophic velocities, Chl concentration, etc.) at the same resolution and location as Level 1 source data; are not on a uniform grid in space or time

Level 3 composite L2-derived geophysical variables binned or interpolated onto uniform space-time grids, e.g., spatial (1km×1km, or 1×1°,…) or temporal (1d, 8d, …) averages

Level 4 model output or results from analyses of lower-level data (e.g., variables derived from multiple measurements like primary production, K490, DOM, PIC, POC, ...) (https://en.wikipedia.org/wiki/SeaWiFS)

For example, to study chlorophyll in the Mediterranean the "Binned Level 3 data" from MODIS (NASA/ESA) at their highest available spatial and temporal resolution of 4.6km × 4.6km and 1/day are often used.

The geophysical quantities available this category are: i) normalised water-leaving radiances in 5 visible wave bands; chlorophyll calculated using a standard bio-optical algorithm (from these radiances) and the attenuation coefficient at 490 nm (idem); 3 types of aerosol-related parameters (Angström exponents and optical thickness).

These data are produced on a regular grid that covers the entire planet. They are composites of Level 2 data (geophysical quantities calculated for each pixel (1km × 1km) of each pass of the satellite sensor (swath 2330 km, 99 min to complete one orbit, yields about 1 value per day for any place on earth) available for a given unit area (21.16 km2) and time interval (1d).

IV – Deriving the Chl concentration

Approach

Several approaches exist to determine Chl concentration from Lw(λ), the reflectance, or the remote sensing reflectance.

First, it is possible to use the values of Lw, R, or Rrs at different wavelengths in the form of ratios (or ratios of differences), and to link these parameter combinations to simultaneously measured *in situ* Chl concentrations using purely empirical relationships. Those are usually called **empirical algorithms**; the most commonly used is the "blue/green" ratio, i.e., the ratio of radiances at wavelengths of about 440 and 550 nm. The use of this particular ratio is of course motivated by the fact that these two wavelengths represent the minimum and maximum absorptions by phytoplankton.

The algorithm becomes **semi-analytical** if it is based on a bio-optical model that includes relationships involving, for instance, IOPs and/or AOPs (such as a and bb, or Kd and b).

The most "fashionable" approach at present is to use neural networks.

[Example: "Seawater-type based neural networks for Ocean Color data inversion", 2013, A. Saptawijaya, D. D'Alimonte, T. Kajiyama. Abstract:

"The retrieval of Ocean Color (OC) data products is here investigated by using Multi Layer Perceptron (MLP) neural nets. Synthetic data have been generated for this scope with a forward OC model. These samples have then been used to train and assess the MLP performance considering different seawater types (WTs) with optical properties driven by: chlorophyll (Chl-a), colored dissolved organic matter (CDOM), and non-pigmented particulate matter (NPPM), as well as a mixture of Chl-a, CDOM and NPPM (denoted MIXI). Acknowledging that MLP classification results represent WT posterior probabilities, an integrated machine learning approach is set up by joining MLPs for data regression and classification in a composite scheme. Results indicate that this approach is valuable to support the use of regional ocean color inversion schemes by decomposing the overall challenge in sub-components, optimally addressing each of them, and combining the individual solutions in a principled framework."]

Wavelengths

Historically, the preferred wavelengths to use in these algorithms are:

443, 520, 550, 670 (20 nm)

as used by the **COASTAL ZONE COLOR SCANNER (CZCS)**, the first ever ocean colour satellite, put into orbit in October 1978 and operational until mid-1986, whose data were used in many groundbreaking studies.

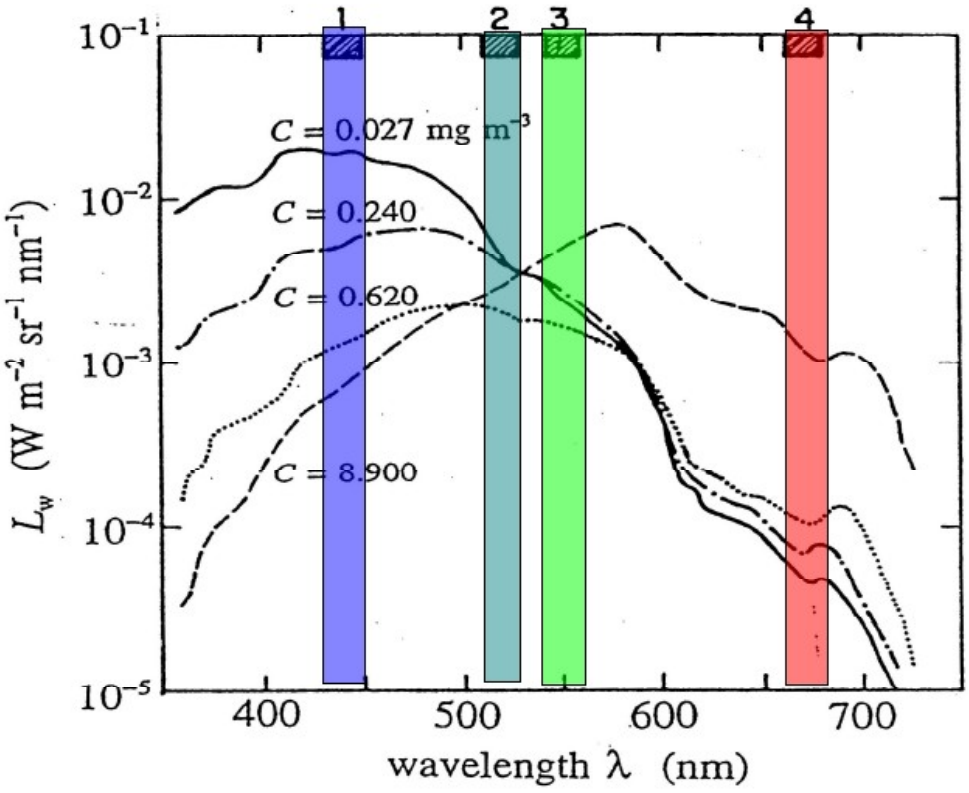

1) 443 nm – 2) 520nm – 3) 550 nm – 4) 670 nm

"In the blue part of the visible spectrum (e.g., at 442 nm), reflectance decreases as [Chl] increases. This is because the maximum absorption by chlorophyll *a* occurs at 442 nm.

Let us recall that the reflectance R varies inversely with the absorption, proportionally to bb/a, where a and bb are the absorption and backscattering coefficients, respectively. In contrast, in the green part of the visible spectrum (e.g., at 555 nm), R increases with increasing [Chl] due mostly to backscattering.

Consequently, the "blue-to-green" reflectance ratio decreases with [Chl]. In practice, log10 ([Chl]) is modelled as a polynomial function of log10 (R442/ R555), which allows its estimation from reflectance measurements."

(Excerpt from Gernez as is the following figure illustrating the subject)

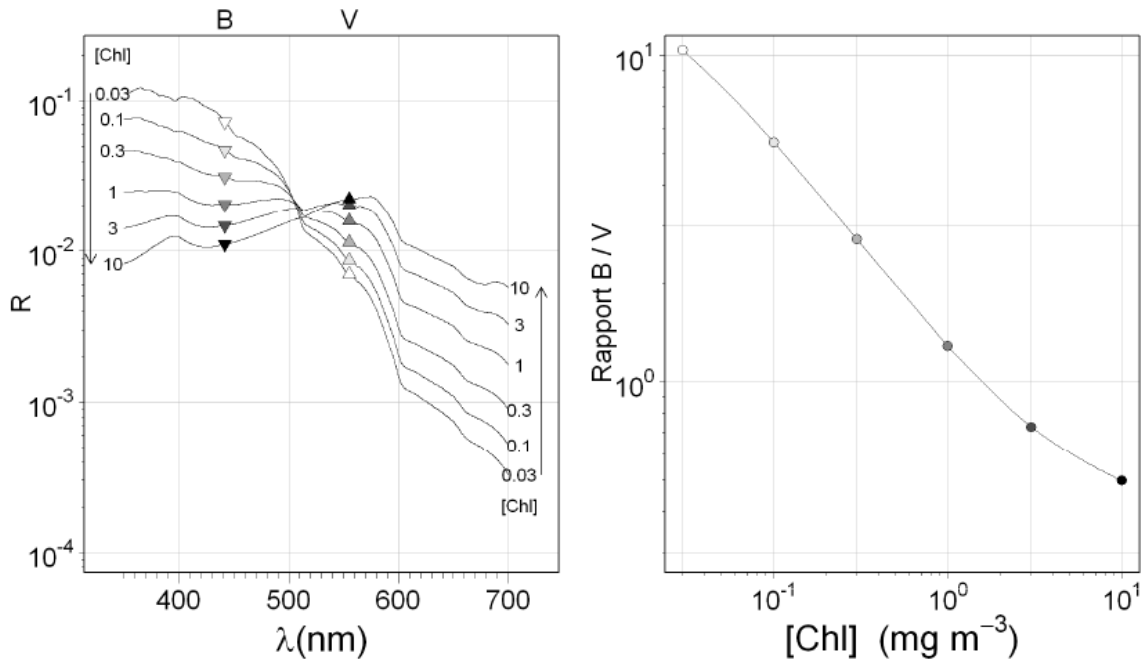

Figure 1-10 Variation modélisée de la réflectance en fonction de la [Chl] : à gauche, spectres de réflectance pour plusieurs niveaux croissant de [Chl] (en mg m^{-3}), montrant la diminution progressive dans le bleu et l'augmentation dans le vert ; à droite, rapport « bleu-sur-vert » R(442) / R(555) en fonction de la [Chl]. Les réflectances ont été modélisées à partir de la [Chl] selon le modèle de Morel et Maritorena (2001).

Below: Examples of wavelengths used in empirical algorithms related to the absorption spectra of the different water constituents
(OCM – Ocean Color Monitor; see appendix).

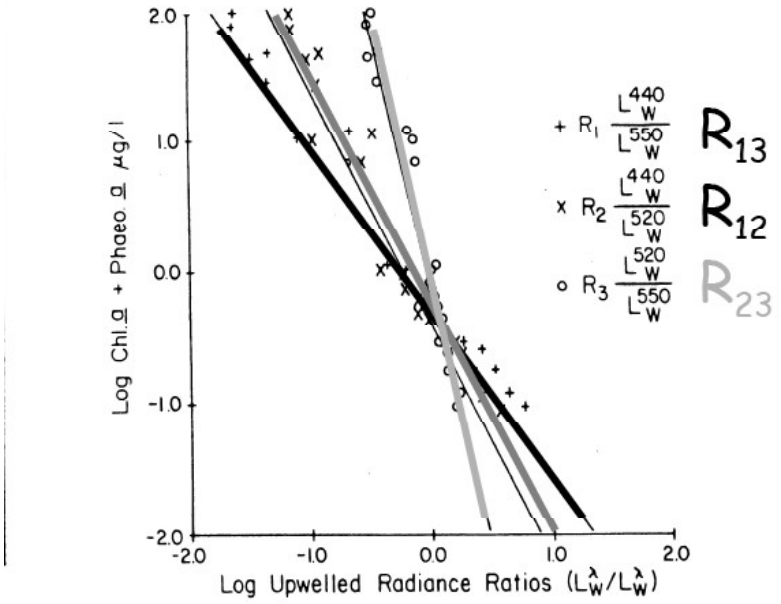

Figure 7.12 Ratios R of upwelling radiance just above the sea surface between pairs of light bands, as a function of the chlorophyll and phaeopigment concentration at the surface. The superscript on L refers to the wavelength in nanometers (from Gordon and Clark, 1980).

Straight lines obtained for log Chla vs the radiance ratios at classical wavelengths

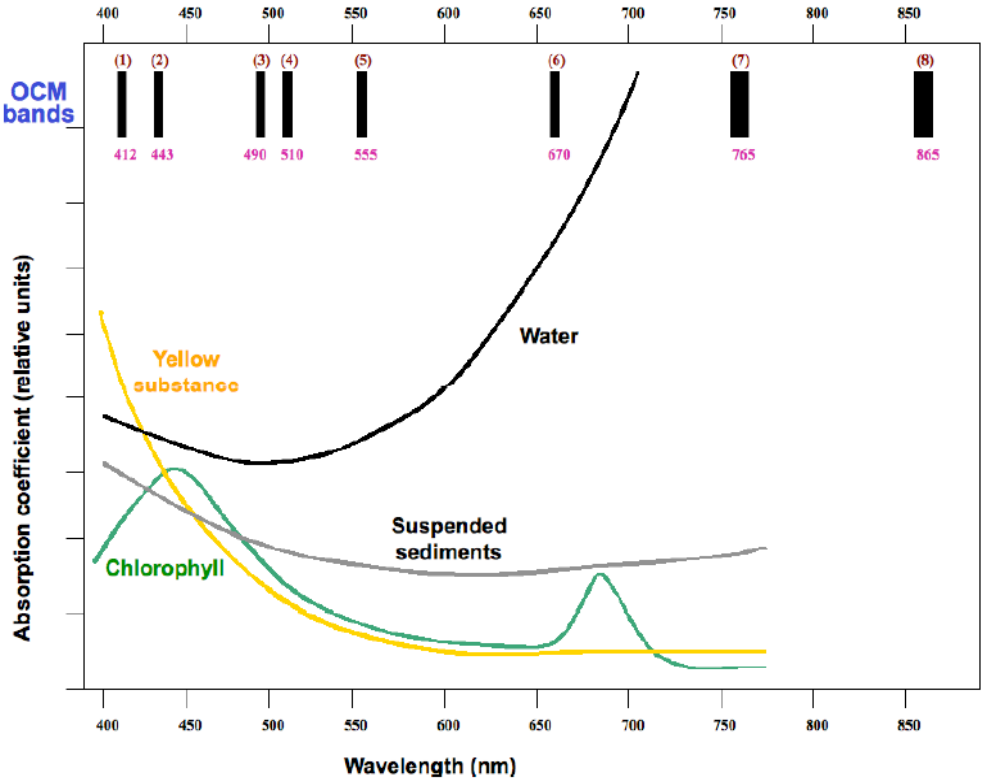

Les algorithmes d'inversion de la [Chl] à partir des mesures de réflectances

Il existe plusieurs approches pour estimer la [Chl] depuis l'espace (Morel et Gordon 1980).

L'approche empirique, initialement développée pour le traitement des données CZCS (Clark 1981) est celle utilisée pour SeaWiFs et MODIS. Les différentes versions des algorithmes OC2, OC3 et OC4 (O'reilly *et al.* 1998) sont basées sur le même principe : établir le meilleur lien statistiques entre des mesures concomitantes de [Chl] et de remote-sensing réflectance R_{rs}. Pour cela, les quantités utilisées sont d'une part, le logarithme de la [Chl] et d'autre part, le logarithme du rapport bleu-sur-vert de réflectance. L'algorithme OC2 (CZCS) utilise comme rapport B /V le rapport $R_{rs}(490)/R_{rs}(555)$, l'algorithme OC3 (MODIS-A) utilise le maximum des rapports $R_{rs}(443)/R_{rs}(551)$ et $R_{rs}(488)/R_{rs}(551)$ et l'algorithme OC4 (SeaWiFs) le maximum des rapports $R_{rs}(443)/R_{rs}(555)$, $R_{rs}490)/R_{rs}(555)$ et $R_{rs}(490)/R_{rs}(555)$. Leur structure générale est :

$$[\mathrm{Chl}] = 10^{\sum_{n=0}^{N} a_n R^n},$$

où N (égal à 3 pour OC2 et 4 pour OC3 et OC4) est le degré du polynôme définis par les coefficients a_n.

L'approche semi-analytique est basée sur un modèle bio-optique faisant intervenir les IOPs a et b_b. Dans un premier temps, les quantités a et b_b (ou plus exactement K_d et b) sont reliées de façon empirique à la [Chl] (par ex. Morel et Maritorena 2001; Loisel et Morel 1998). Dans un deuxième temps, les réflectances sont calculées à partir de a et b_b. L'algorithme OC4Me (MERIS) utilise les longueurs d'ondes (443, 490, 510 et 560 nm) et le rapport de réflectances R (pour un soleil au zénith) au lieu des remote sensing réflectances R_{rs} (Morel et Antoine 2007).

L'intérêt de l'approche semi-analytique est qu'il est possible de modéliser toutes les propriétés optiques (dont la R_{rs}) à toutes les longueurs d'onde, ce qui permet la comparaison avec les algorithmes empiriques. Comme le montre la figure ci-dessous, les deux approches donnent des résultats similaires (Morel *et al.* 2007c).

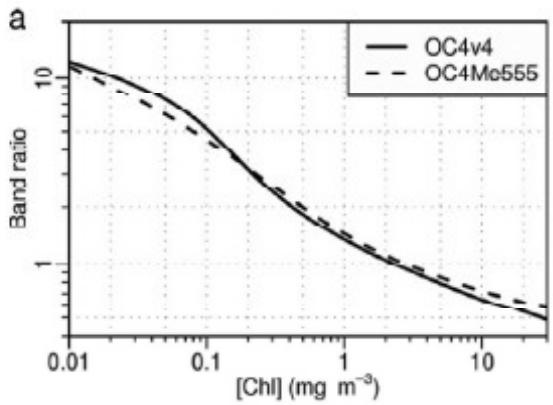

Extrait de Morel et al. (2007). Représentation graphique des algorithmes d'inversion de la [Chl] à partir du rapport de réflectance : en continu OC4v4 et en tireté son équivalent de type OC4Me.

(courtesy P. Gernez, excerpt from thesis 2009)
Careful, in the equation Chl depends on polynomials with Rrs and not with R (except OC4Me)

Examples of empirical algorithms

For OCTS (Kishino et al., 1998)

Chla (mg/m^{-3}) = 0,2818[(Lw(520)+Lw(565))/Lw(490)]$^{3.497}$

For OC2 (O'Reilly et al., 1998)

Chla (mg m^{-3}) = $10^{a_0+a_1\rho+a_2\rho^2+a_3\rho^3} + a_4$

with ρ **= log10(Rrs(490)/Rrs(555))**

a0 = 0.341; a1 = -3.001; a2 = 2.811; a3 =-2.041; a4 = -0.04

if Rrs(555) is no available it van be obtained from Rrs(565) for POLDER

Rrs(555)=1.0628Rrs(565)+0.0015

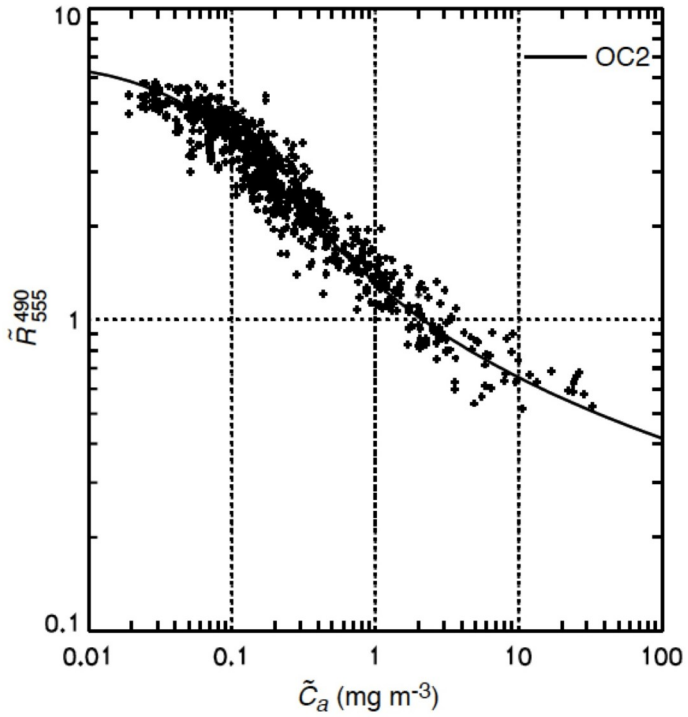

Fig. 1. A scatterplot of $\tilde{R}^{490}_{555}$ versus $\tilde{C}_a$ for the original SeaBAM data set ($N = 919$). The curve represents the OC2 algorithm.

(from O'Reilly et al., 2000, NASA Technical Memorandum 2000-206892, Vol 11)

For OC2v2 (O'Reilly et al., 2000)

Chla (mg m^{-3}) = $10^{a_0+a_1\rho+a_2\rho^2+a_3\rho^3} + a_4$

with ρ **= log10(Rrs(490)/Rrs(555))**

a0 = 0.2974; a1 = -2.2429; a2 = 0.8358; a3 =-0.0077; a4 = -0.0929

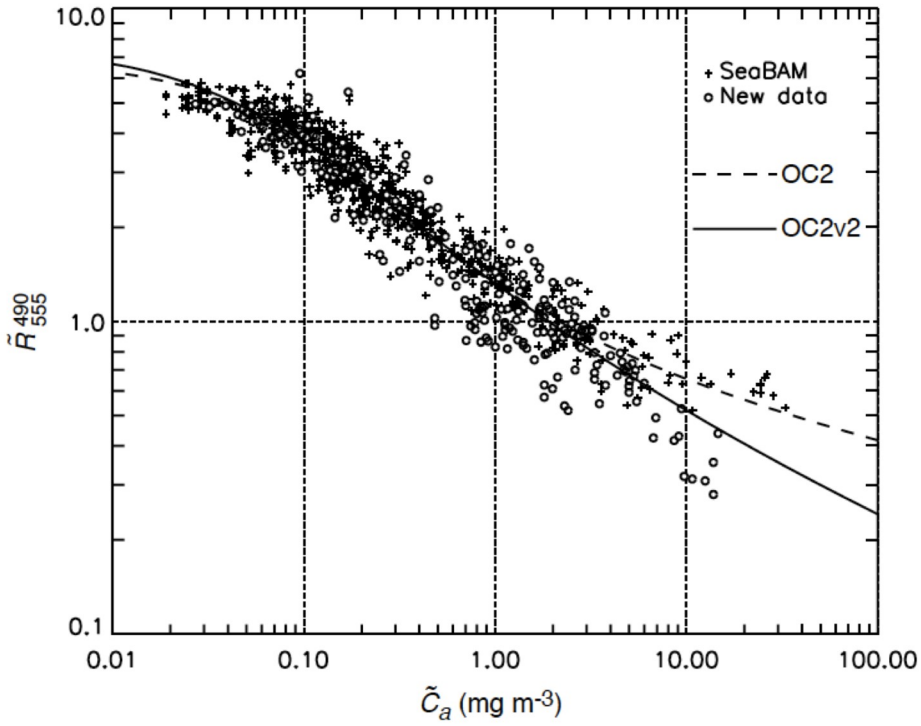

Fig. 2. A scatterplot of $\tilde{R}^{490}_{555}$ versus $\tilde{C}_a$ for the original SeaBAM (crosses) and the new data (circles). The dotted curve represents the original OC2 algorithm; the solid curve represents OC2v2, the new algorithm.

(from O'Reilly et al., 2000, NASA Technical Memorandum 2000-206892, Vol 11)

For OC4v4 (O'Reilly et al., 2000)

$$\text{Chla (mg m}^{-3}) = 10^{a_0 + a_1\rho + a_2\rho^2 + a_3\rho^3 + a_4\rho^4}$$

with ρ = log10(Rrs(λ)/Rrs(555))
a0 = 0.366; a1 = -3.067; a2 = 1.93; a3 =-0.649; a4 = -1.532
and Rrs(λ) = the maximum of Rrs(443), Rrs(490), and Rrs(510)

Bricaud(2002) for the Mediterranean

$$\text{Chla} = 2.094[R(443)/R(555)]^{-2.357}$$

Volpe et al. (2007) for the Mediterranean

$$\text{Chla (mg m}^{-3}) = 10^{a_0 + a_1\rho + a_2\rho^2 + a_3\rho^3 + a_4\rho^4}$$

with ρ = log10(Rrs(λ)/Rrs(555))
a0 = 0.4424; a1 = -3.686; a2 = 1.076; a3 = 1.684; a4 = -1.437
and Rrs(λ) = the maximum of Rrs(443), Rrs(490), and Rrs(510)

A good summary of the algorithms can be found in (also mentioned in Chapter 5 and available from the OPB305 website):

Werdell P. Jeremy, Franz B.A, Bailey SW, Feldman GC, Boss E, Brando VE, Dowell M, Hirata T, Lavender SJ, Lee Z, Loisel H, Maritorena S, Mélin F, Moore TS, Smyth TJ, Antoine D, Devred E, d'Andon OH, Mangin A.
Generalized ocean color inversion model for retrieving marine inherent optical properties.
Appl Opt. 2013 Apr 1;52(10):2019-37. doi: 10.1364/AO.52.002019.

Ocean color measured from satellites provides daily, global estimates of marine inherent optical properties (IOPs). Semi-analytical algorithms (SAAs) provide one mechanism for inverting the color of the water observed by the satellite into IOPs. While numerous SAAs exist, most are similarly constructed and few are appropriately parameterized for all water masses for all seasons. To initiate community-wide discussion of these limitations, NASA organized two workshops that deconstructed SAAs to identify similarities and uniqueness and to progress toward consensus on a unified SAA. This effort resulted in the development of the generalized IOP (GIOP) model software that allows for the construction of different SAAs at runtime by selection from an assortment of model parameterizations. As such, GIOP permits isolation and evaluation of specific modeling assumptions, construction of SAAs, development of regionally tuned SAAs, and execution of ensemble inversion modeling. Working groups associated with the workshops proposed a preliminary default configuration for GIOP (GIOP-DC), with alternative model parameterizations and features defined for subsequent evaluation. In this paper, we: (1) describe the theoretical basis of GIOP; (2) present GIOP-DC and verify its comparable performance to other popular SAAs using both in situ and synthetic data sets; and, (3) quantify the sensitivities of their output to their parameterization. We use the latter to develop a hierarchical sensitivity of SAAs to various model parameterizations, to identify components of SAAs that merit focus in future research, and to provide material for discussion on algorithm uncertainties and future ensemble applications.

Utilised vocabulary:

GIOP – DC	generalized IOP (GIOP) model – Default Configuration
NOMAD	NASA bioOptical Marine Algorithm Data set (Bailey and Werdell, 2006)
SAA	Semi-analytical algorithm

V – Example of a "generalised" algorithm to obtain the suspended matter concentration in coastal waters

From *Ouillon et al., Sensors, **2008**, 8, 4165-4185; DOI: 10.3390/s8074165*
Optical Algorithms at Satellite Wavelengths for Total Suspended Matter in Tropical Coastal Waters

Proposal for a global algorithm with threshold
In an attempt to build a better global algorithm, we thus propose to merge the two best-performing relationships in one formulation, following:

(a) turbidity is calculated using algorithm 2:

$$Turb = - 6204217\ (Rrs681)^3 + 179652\ (Rrs681)^2 + 36.49\ Rrs681 + 0.452 \quad (6)$$

(b) if the resulting turbidity < 1 FTU, its calculation is replaced by algorithm 6:

$$Turb = 90.647\ (Rrs620.Rrs681/Rrs412)^{0.594} \quad (7)$$

As this algorithm is based on three wavelengths (412, 620 and 681 nm, available e.g. with MERIS), we propose to call it hereafter TURB3. Its statistical performances show its ability to estimate turbidity with a mean bias of 3.6%, a rms error of 35% and a mean quadratic error of 1.4 FTU (Table 3, Fig. 12). Algorithm 6 induces lower rms errors both globally and in New Caledonia, but fails to estimate higher turbidity (as indicated by higher rms errors in Cuba and Fiji). TURB3 enables to significantly reduce the mean quadratic error with the Fiji data (2.4 FTU against 3.7 with algorithm 6).

Figure 12. Comparison of measured turbidity (averaged over 3 m below the sea surface) and turbidity calculated from Rrs412, Rrs620 and Rrs681 using TURB3 algorithm (N=193).

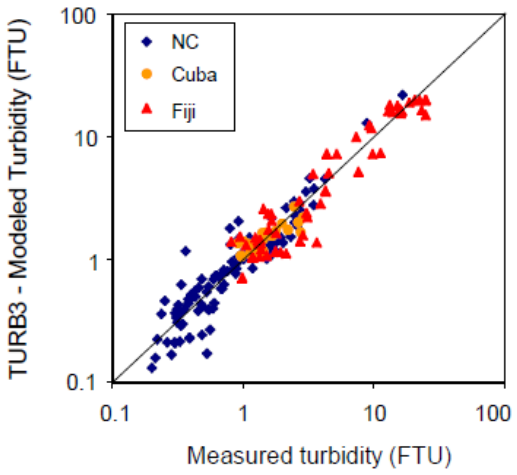

*FTU: Formazine Turbidity Unit (unit for calibrating turbidometers)

For coastal waters, also see these (non-exhaustive list):

“Remote Sensing of Coastal Waters” by N. Hoepffner, G. Zibordi, in Encyclopedia of Ocean Sciences (Second Edition), 2009

“Regional Algorithms for European Seas: A Case Study Based on MERIS Data”, 2013, IEEE Geoscience and Remote Sensing Letters, Tamito Kajiyama, Davide D'Alimonte, Giuseppe Zibordi

with the following abstract: Advances in satellite ocean color technologies and methodologies are expected to lead to the generation of coastal water bio-optical products with accuracies close to those targeted for oceanic regions. In view of contributing to such a progress, multilayer perception neural networks complying with standard Medium Resolution Imaging Spectrometer (MERIS) pigment indices were developed relying on regional highly accurate in situ data. This work illustrates and discusses the application to sample MERIS imagery of those neural networks trained to produce pigment indices in seas characterized by increased levels of bio-optical complexity: the Baltic, the Northern Adriatic, and the Western Black Seas.

V – Regional algorithms for the Mediterranean

A partir de mesures effectuées le 22 juillet 1992 au large de Gaza, Gitelson et. al (1996) proposèrent le 1er algorithme régional. Il s'agit d'une adaptation du modèle global développé pour les eaux du cas 1 par Gordon et Morel (1983) :

$$[\mathrm{Chl}] = 0.914 \left[\frac{R(442)}{R(550)}\right]^{-1.86}.$$

Cet algorithme a été validé par des mesures en Méditerranée orientale entre juillet 1981 et juin 1984 (Berman *et al.* 1984).

A partir des mesures réalisées sur l'ensemble du bassin dans le cadre de l'expérience « SYnoptic Mesoscale and PLankton EXperiment » SYMPLEX (1998-2000), D'ortenzio *et al.* (2002) proposèrent un algorithme régional du type OC2 :

$$[\mathrm{Chl}] = 10^{(0.217-2.728R+0.704R^2+0.297R^3)} - 0.035, \text{ où } R = \log_{10}\left[\frac{R_{rs}(490)}{R_{rs}(555)}\right].$$

Cet algorithme est basé sur des mesures acquises dans des zones en majorité oligotrophes (70% des [Chl] < 0.1 mg m^{-3}) ; il a été forcé afin de reproduire les valeurs dérivées de l'algorithme OC2 pour les plus fortes concentrations de [Chl].

A partir de mesures effectuées en septembre 1999 en mer Ionienne et en Méditerranée Occidentale (campagne PROSOPE), entre décembre 1997 et janvier 1998 en mer d'Alboran (campagne ALMOFRONT-2), Bricaud *et al.* (2002) proposèrent :

$$[\mathrm{Chl}] = 2.094 \left[\frac{R(443)}{R(555)}\right]^{-2.357}.$$

Cet algorithme a été validé par les mesures effectuées entre novembre 1996 et juin 1997 à la station DyFaMed et entre mars et juillet 1998 dans le bassin Algérien (campagnes ELISA-3 et -4).

L'algorithme régional le plus récent est le « MedOC », développé par Volpe *et al.* (2007) à partir de données assemblées sur plus de 30 campagnes entre 1997 et 2005 dans l'ensemble du bassin. C'est une adaptation de l'algorithme OC4 :

$$[\mathrm{Chl}] = 10^{(0.4424-3.686R+1.076R^2+1.684R^3-1.437R^4)},$$

where $R = \log_{10}(\max(Rrs(443)/Rrs(555), Rrs(490)/Rrs(555), Rrs(510)/Rrs(555))$

(courtesy P. Gernez, excerpt from Thesis, 2009)

En Méditerranée, dans les eaux claires, comme cela est montré sur la figure5-2, le rapport bleu-sur-vert de réflectance est généralement situé au dessous de la loi moyenne (Gitelson *et al.* 1996 ; Bricaud *et al.* 2002 ; D'ortenzio *et al.* 2002 ; Claustre *et al.* 2002b ; Volpe *et al.* 2007). En conséquence, les algorithmes d'inversion basés sur un rapport de réflectance surestiment la concentration en chlorophylle réelle. Cela est illustré en figure 5-3 où l'erreur d'estimation au site BOUSSOLE est indiquée sur des exemples de cartes satellites (SeaWiFs) de [Chl] à six dates choisies entre 2001 et 2006. C'est ce qu'on appelle l'**anomalie de réflectance**, ou **anomalie de chlorophylle**, ou encore **anomalie bio-optique en Méditerranée**.

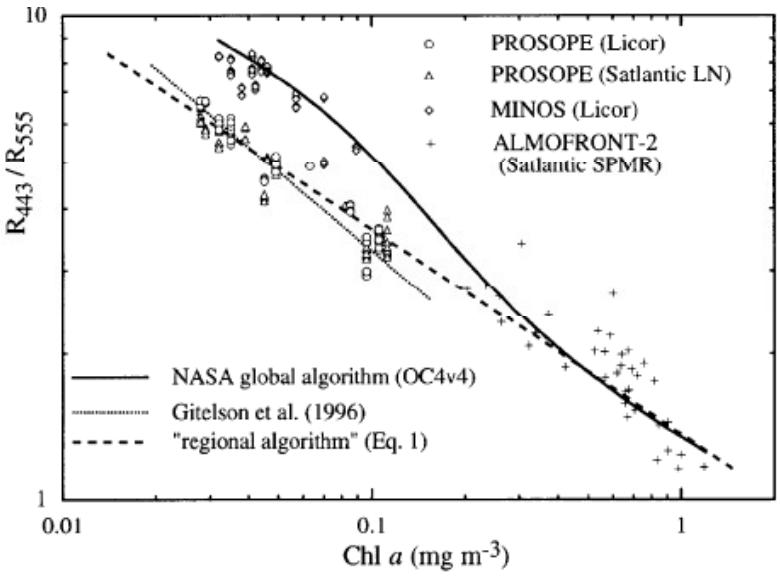

Figure 5-2 Extraite de Bricaud et al. (2002).Variations du rapport R(443)/R(560) en fonction de la [Chl]. Les mesures furent réalisées lors de diverses campagnes, comme indiqué. La ligne continue représente l'algorithme standard OC4v4 de la NASA. Les tiretés et les pointillés indiquent les algorithmes régionaux de Bricaud et al. (2002) et Gitelson et al. (1996).

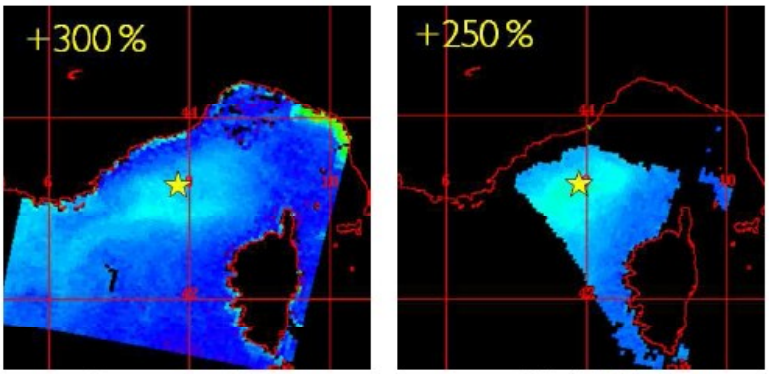

2 septembre 2001
[Chl] = 0.05 mg m^{-3}

29 juin 2005
[Chl] = 0.085 mg m^{-3}

Figure 5-3 Extract from the presentation "Nuances in case 1 waters optical properties: a case study in the oligotrophic northwestern Mediterranean Sea (BOUSSOLE site)" D. Antoine and A. Morel, Ocean Optics XVIII, Montreal, October 9-13, 2006. Examples of satellite images (SeaWiFs, NASA GSFC) of the Ligurian Sea on two specific dates in 2001 and 2005. The BOUSSOLE site is indicated by a star: the chlorophyll concentration was obtained by HPLC. The error estimate is given in yellow at the top left.

Several hypotheses have been put forward to explain this anomaly. According to Gitelson *et al.* (1996), the overestimation of [Chl] is linked to an excess in the specific attenuation cp* due to the presence of coccolithophores and nomadic coccoliths. However, the typical coccolithophorid abundances to small to explain any differences in scattering (d'Ortenzio et al. 2002). Another hypothesis attributes the higher backscattering at 555 nm to the presence of aerosols from the Sahara (Claustre et al. 2002b), but to date there is no direct evidence of desert dust deposition on the sea surface altering the ocean's optical properties. More recently, it was shown that Mediterranean waters are characterized by an excess absorption in the blue part of the visible spectrum due to above average absorption by dissolved substances (Morel et al., 2007a; Morel 2009; Morel and Gentili, 2009).

The development of regional algorithms has made it possible to correct estimation errors for [Chl] on several occasions (Gitelson et al. 1996; Bricaud et al. 2002; d'Ortenzio et al. 2002; Volpe et al. 2007). These regional algorithms were constructed empirically, i.e., based on data collected over a certain time interval and for certain areas. Their validity beyond these geographical and temporal limits is therefore by no means guaranteed.

To summarize, the availability of global data made it possible to establish laws that describe the mean values of certain variables. A systematic bias has been reported for the Mediterranean, in that the reflectance ratio B/V in clear waters ([Chl] <0.3 mg m-3) is lower than expected. Consequently, standard remote sensing algorithms tend to overestimate [Chl].

Such overestimations were in fact mainly reported at the end of campaigns that took place in summer (e.g., MINOS in June, AOPEX in August, PROSOPE in September). The situation is different in autumn and winter when [Chl] tends to be underestimated as highlighted by the analysis of time series data from BOUSSOLE station (Gernez thesis, 2009).

During autumn/winter, the B/V ratio is above average and the chlorophyll concentration tends to be underestimated. Gernez (Thesis 2009) hypothesized that there may be seasonal cycles in the bio-optical relationships that create deviations from the global average. "Positive" anomalies (higher B/V ratios and subsequent overestimation of [Chl]) are generated at the outset of water column stratification and therefore observed in summer. "Negative" anomalies (low B/V ratios and underestimation of [Chl]) are observed in autumn as the summer stratification starts to break down and transitions to the winter mixed regime which would result in a lower backscattering (compared to the global averages).

The regional model by Volpe et al. (2007) describes the positive anomalies very well. However, its systematic use would lead to significant underestimations of [Chl].

VI – Model for French coastal waters

There is also the so-called OC5 model (Gohin et al., 2002), a bio-empirical model using MODIS, MERIS and SeaWifs data that has been adapted to French Case 2 coastal waters. This algorithm tends to correct the overestimation of chlorophyll in turbid waters (e.g., the Rhone River plume) using a table of empirical measurements (lookup table) adapted to the French Channel coasts based on Rrs thresholds at 555 nm and 412 nm. This algorithm also gives good results in the Gulf of Lion.

* Gohin, F., Druon, J.-N. and Lampert, L. (2002) A five channel chlorophyll algorithm applied to SeaWifs data processed by SeaDas in coastal waters, International journal of remote sensing, vol. 23, pp. 1639-1661

The applicability of which has also been tested for coastal areas around the globe:

David Dessailly (2016). GlobCoast Moyenne mensuelle de la chlorophyll-a (chl-a OC5). Université du Littoral Côte d'Opale - Laboratoire d'Océanologie et de Géoscience. http://doi.org/10.12770/3274ed9f-5dc1-4613-98f1-e4f59fabe05b

Monthly mean chlorophyll-a (for period 2002-2012) after Gohin (2002) for coastal waters, using MERIS data with POLYME atmospheric corrections of the Hygéos POLYMER algorithm (Steinmetz, 2011).

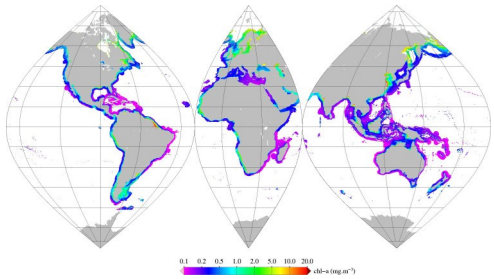

The “coastal zone” used in this analysis sometimes extends beyond what would normally be defined a coastal zone (based on the bathymetry) and extends for instance into the mainly oligotrophic waters of the Mediterranean where these algorithms reach their limits in terms of validity.

SEXTANT Infrastructure of geographical terrestrial and marine data
https://sextant.ifremer.fr/record/3274ed9f-5dc1-4613-98f1-e4f59fabe05b/

Other refs:
Gohin, F., 2011. Annual cycles of chlorophyll-a, non-algal suspended particulate matter, and turbidity observed from space and in-situ in coastal waters. Ocean Science 7, 705–732.

Gohin, F., Saulquin, B., Bryere, P., 2010. Atlas de la Température, de la concentration en Chlorophylle et de la Turbidité de surface du plateau continental français et de ses abords de l’Ouest européen. Ifremer.
URL http://archimer.ifremer.fr/doc/00057/16840/

Bear in mind that the use of a regional algorithm can be dangerous because while it may improve the estimates for some particular season, it may perform worse than a more global algorithm during other seasons.

Currently, we are observing a transition towards the detection of mesoscale (10 to 100 km) to sub-mesoscale (1 to 10 km) physical structures.

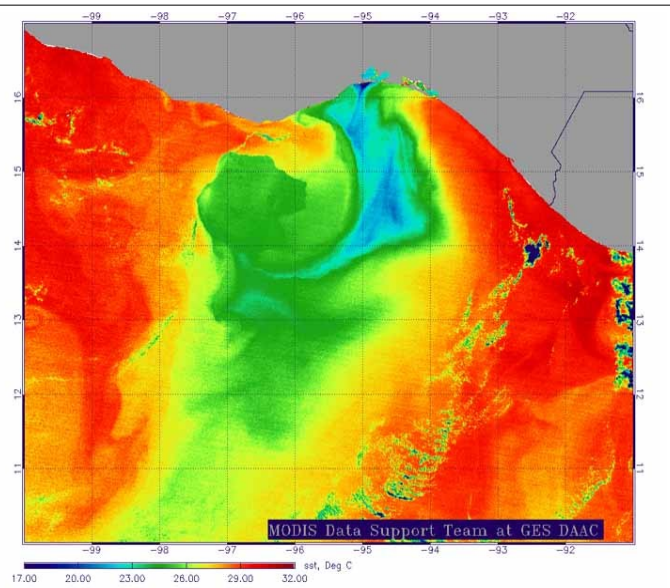	**MODIS Sea Surface Temperature, 2000 December 6, 17:05**
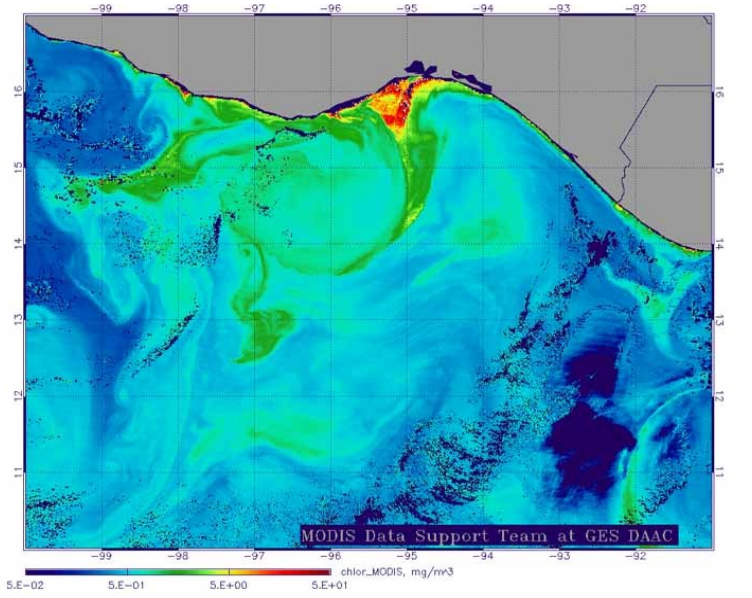	**MODIS Surface Chlorophyll Concentration, 2000 December 6, 17:05**

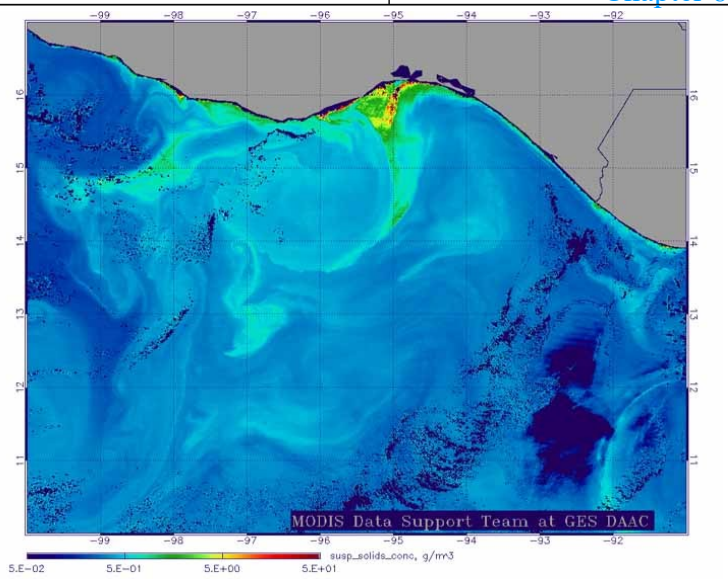

MODIS Total Suspended Solids, 2000 December 6, 17:05

Example: detection of Sargassum

D. Teixeira Da Silva, A. Ody, D. Nerini, A. Petrenko, A. Minghelli, J.-M. André, L. Berline, *Spectral properties of Sargassum reflectance spectra: relationships with Sargassum fractional coverage and depth*, Ocean Optics, Oct 2018

Sargassum project at MIO also involving C. Chevalier, C. Pujol, T. Changeux, etc.

Context : Pelagic Sargassum

Context : Massive pelagic Sargassum strandings in the NTA coasts

- Since 2011 => Causing large ecological, economical and societal damages

-

Context : Sargassum quantification, a remote-sensing challenge

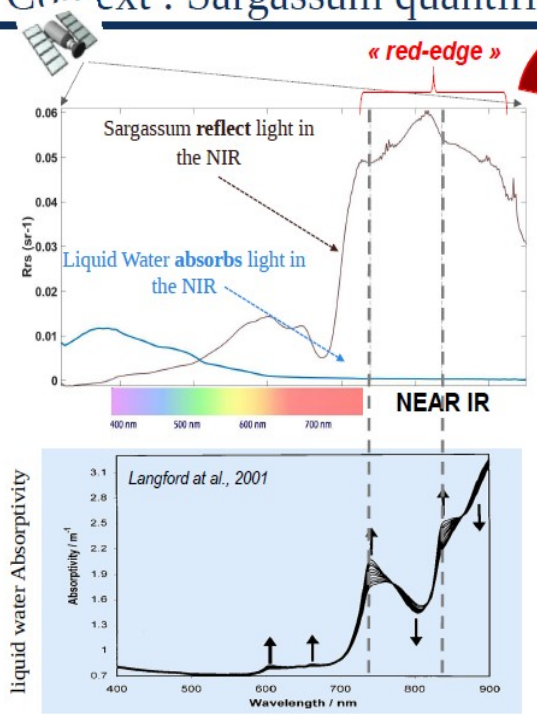

Algae Spectral Index
« red-edge »
e.g.

FAI/AFAI
(Alternative/ Floating algae Index)
Hu 2009; Wang et Hu, 2016

MCI
(Maximum Chlorophyll Index)
Gower *et al.*, 2005

The **water proportion** inside the pixel but also the presence of water above the Sargassum rafts (**depth**) will impact the Sargassum signal in the NIR and thus the algae index values.

Actual Sargassum quantification methods are mainly based on relationships between index and Sargassum proportion or density biomass (e.g. Wang and Hu, 2016, Qi et a Xing et al., 2017, Wang et al., 2018)

Methods: In situ dataset

- Reflectance measurements from the ship deck: Sargassum in their natural environment for various proportions and depths

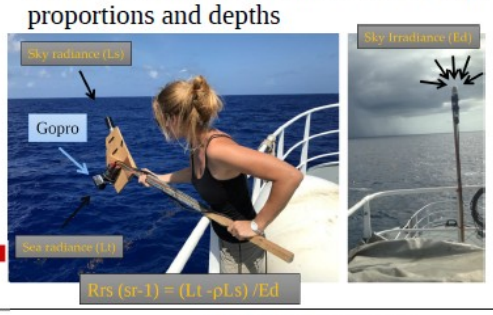

- ✓ Hyperspectral TRiOS RAMSES radiometers (320-950 nm) (protocol: Ruddick et al., 2006)
- ✓ GOPRO to take pictures of the sampling area

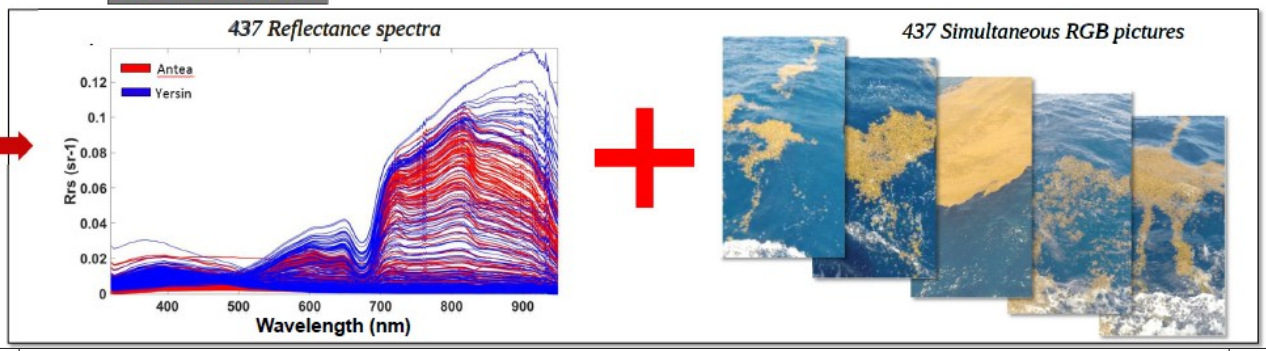

Two Antea campaigns in June/July 2017 and Yersin in Oct 2017 (MIO)

Our goal is to take into account the proportion of Sargassum in each pixel at their specific depth.
E.g., 100% Sargassum but at various depths:

Methods: Reference Dataset

- Measurements in a dark bucket for a Sargassum Proportion of 100 % and various known depths.

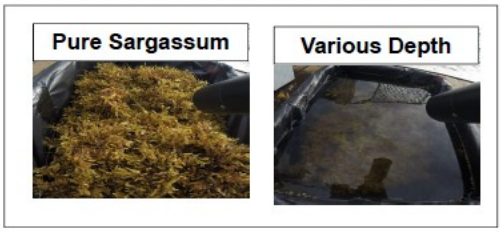

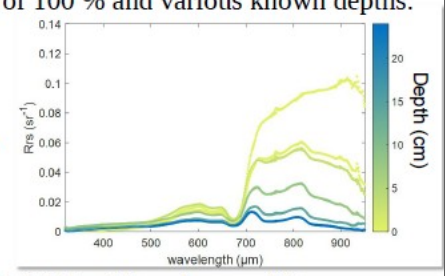

- Spectra used in a linear mixing model (Rrs=P * RrsSarg + (1-P)*RrsWater) to model spectra at ea depth for Proportions from 0 to 100%

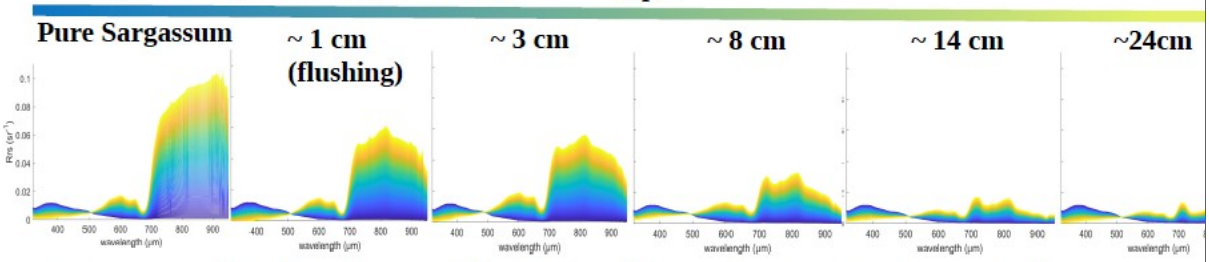

- Compute relationships between Algae Index and Proportion for various known depths

Summary

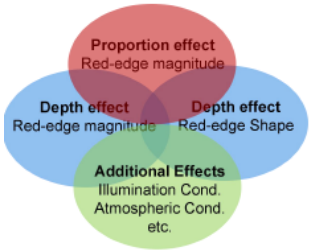

- The relationships between Algae Index (at least AFAI and MCI) an Proportion appear to be very complex and scattered because of the effects.
  - → Multiple proportion values for a given index value, depending depth.
- Need to estimate the Sargassum raft depth:
  - ✓ through liquide water absorption band intensity ?
  - ✓ through relationship with wind and sea states ?
- PCA analysis shows that:
  - ✓ We can describe the Sargassum reflectance spectra shape with only 3 principal components.
  - ✓ PC1 allows estimating the Proportion independently from the red-edge reflectance and possibly from the depth effects

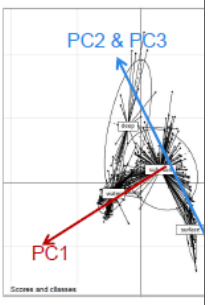

- Remote Sensing applications: Spatial resolution, Spectral resolution, atmospheric conditions, etc...

VII - APPENDICES Instruments used in marine remote sensing

For more up-to-date information, see the latest conference:

https://oceanopticsconference.org/

(Ocean Optics XXV should have taken place in October 2020 but was postponed till autumn 2022 due to the COVID pandemic)

Description of satellites based on the product they deliver:
http://www.ceos.org/
Committee on Earth Observation Satellites

E.g., **Name of carrier satellite** (name of sensor; not always given)

1) MW and HF/VHF radars

- scatterometere → SSW

ex **Seasat, ERS-1 (2), ADEOS (2), Quikscat**

- SAR → waves, dynamic structures, SSW, patches

ex **Seasat** (SAR), **Cosmos, ERS-1 (2), Radarsat, Envisat** (ASAR)

- Altimeter → dynamic topography, SSW, SSH

ex **GEOS-3, Seasat, Geosat, ERS-1 (2), Topex-Poseidon, Jason-1 (2), Envisat**

[Not on satellite:
HF/VHF ground radar, CODAR → currents, wave spectra]

2) V/NIR radiometers – high resolution
→ turbidity, fronts, patches, bathymetry, thermal structures (only Landsat)
e.g., **Landsat, Spot** (HRV, HRVIR), **Adeos** (Avnir), **MOS, Resurs**

3) V spectroradiometers – medium/low resolution

→ water colour: chlorophyll, turbidity
(+SST for MODIS)

e.g., **Nimbus** (CZCS) , **IRSP-3 (4), Adeos (2)** (OCTS, POLDER), **Seastar** (SeaWiFS), **Terra-EOS et Aqua-EOS**(MODIS), **Envisat** (MERIS), **ADEOS II** (GLI), NPP (VIIRS), Sentinel 3A (OLCI),
regional: GOCI (Korea), HICO (USA)

4) IR/MW radiometers – low resolution

→ SST

e.g., **NOAA** (AVHRR), **MOS, ERS**
The new generation SEVIRI sensor is a scanning radiometer and it is the rotation of the satellite about its main axis of inertia which is used to acquire the images. 12 channels of visible, mid-infrared and thermal infrared every 15 minutes, with increased spatial resolution.

5) MW radiometers

→ SST, SSW

e.g., **Seasat** (SMMR), **Nimbus** (SMMR), **DMSP, Mir**

6) others

- rotating radar (MIROS, VAGSAT) →waves
- INSAR →currents, waves
- lidar → bathymetry + DOM, Chl
- salinometer (OSIRIS NASA, MIRAS CNES) → SSS
- MW radiometer + interferometer (SMOS 2007) → SSS
- bi-static GPS → SSW, SSS, waves

Acronyms:

AVHRR = Advanced Very High Resolution Radiometer
ASAR = active SAR
CZCS = Coastal Zone Color Scanner
HRV = High Resolution Visible
IR= *infrared (1.3 μm - 1mm)*
MERIS = MEdium Resolution Imaging Spectrometer (300 m)
MODIS = Moderate Resolution Imaging Spectroradiometer (250m, 500 m, 1km)
MW= *microwaves (1 mm - 1m)*
NIR= *near infrared (.7-1.3 μm)*
OCTS = Ocean Color and Temperature Scanner
POLDER = POLarization and Directionality of the Earth's Reflectance
SeaWiFS = Sea-viewing Wide Field-of-view Sensor (1.1 km; 4 km)
SAR = Synthetic Aperture Radar
SMMR = Scanning Multichannel Microwave Radiometer
SSH = *sea surface height*
SSS = *sea surface salinity*
SSW = *sea surface wind*
V = *Visible (.4-.7 μm)*

The satellite-based instruments listed on this page are operational instruments currently used in CMEMS products. Even more satellite observations are used by CMEMS, for climatology, reanalysis and validation purposes, from past missions or from satellites that do not deliver data in real-time.

Instrument type	Ocean parameter measured	Instrument name	Satellite
Spectroradiometer	•Chlorophyll content •Organic and mineral content •Sea surface temperature •Sea Ice Cover	MODIS MERIS	
Infrared radiometer	•Sea surface temperature (SST)	AVHRR AATSR MODIS SEVIRI GOES	(NOAA, USA) + METOP (Eumetsat, Europe) Envisat (ESA, Europe) Aqua, Terra (NASA, USA) MeteoSat (Eumetsat, Europe) (NOAA, USA) DMSP (NASA, USA)
Microwave radiometer	•Atmospheric water vapour content •Atmospheric water liquid content (cloud) •Rain rates •Sea-ice concentration, type, extent •SST •Salinity	SSM/I TMI AMSR-E MWR JMR, AMR	DMSP (NASA, USA) TRMM (NASA, USA) Aqua (NASA, USA) + (developed by JAXA, Japan) Envisat (ESA, Europe) Jason-1, Jason-2 (Cnes, France + NASA, USA)
Altimeter	•Sea-surface height •Ocean surface wind speed •Wave height •Sea ice	Poseidon-2 RA-2 Poseidon-3	Jason-1 (CNES, France + NASA, USA) Envisat (ESA, Europe) Jason-2 (CNES, France + NASA, NOAA, USA + Eumetsat, Europe)
Scatterometer	•Wind speed and heading (10 m above ocean surface) •Rain •Sea ice concentration	ASCAT	Metop (Eumetsat, Europe)
Synthetic Aperture Radar (SAR)	•Wind •Surface wave field •Sea ice monitoring		Radarsat-1, Radarsat-2, Canada Envisat, Europe

(site : http://marine.copernicus.eu/training/education/observation/satellites/)

European Commission <http://marine.copernicus.eu/>
CMEMS=
Copernicus Marine Environment Monitoring Service
providing products and services for all marine applications

o Training & Education
<http://marine.copernicus.eu/training/>
+ online tutorials
<http://marine.copernicus.eu/training/online-tutorials/>

o Ocean State Report

<http://marine.copernicus.eu/science-learning/ocean-state-report/>
+ Ocean State Report 2016 – 1st issue
<http://marine.copernicus.eu/science-learning/ocean-state-report/ocean-state-report-2016-1st-issue/>

o Education

<http://marine.copernicus.eu/training/education/>
+ Observation
<http://marine.copernicus.eu/training/education/observation/>
Satellites
<http://marine.copernicus.eu/training/education/observation/satellites/>
In situ
<http://marine.copernicus.eu/training/education/observation/in-situ/>
+ Modelling
<http://marine.copernicus.eu/training/education/modelling/>
+ Ocean parameters
<http://marine.copernicus.eu/training/education/ocean-parameters/>
Temperature
<http://marine.copernicus.eu/training/education/ocean-parameters/temperature/>
Salinity
<http://marine.copernicus.eu/training/education/ocean-parameters/salinity/>
Currents
<http://marine.copernicus.eu/training/education/ocean-parameters/currents/>
Sea ice
<http://marine.copernicus.eu/training/education/ocean-parameters/sea-ice/>
Sea level
<http://marine.copernicus.eu/training/education/ocean-parameters/sea-level/>
Wind
<http://marine.copernicus.eu/training/education/ocean-parameters/wind/>
Biogeochemistry
<http://marine.copernicus.eu/training/education/ocean-parameters/biogeochemistry/>

Names of NASA present and upcoming missions (2011);

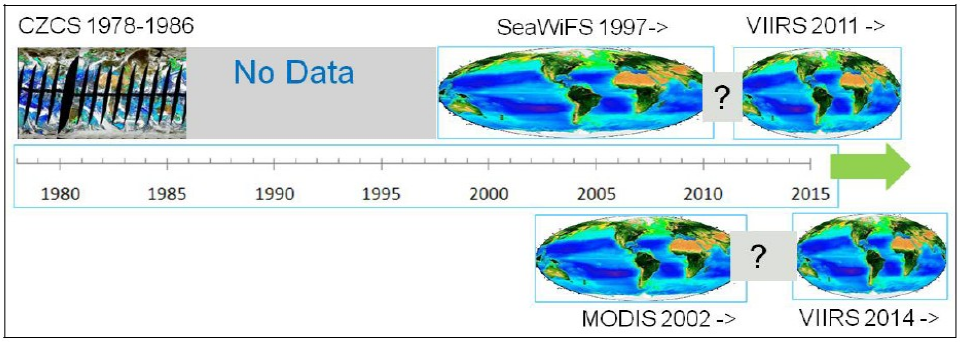

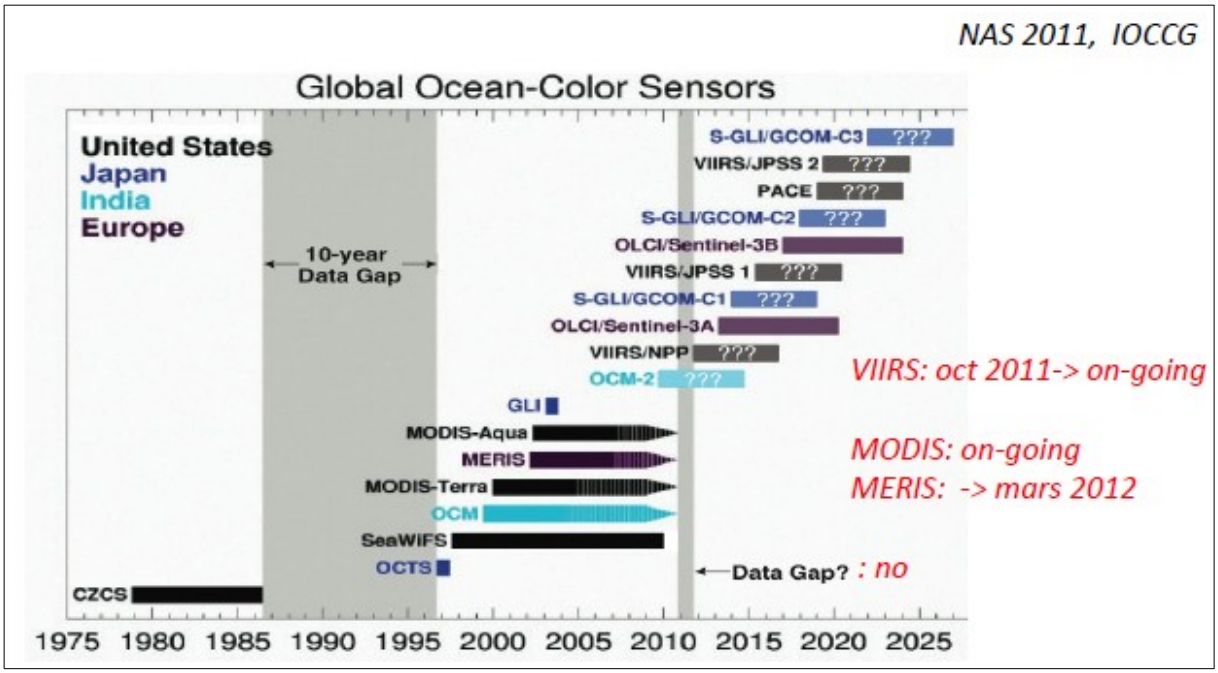

Presentations from IOCS Meeting Lisbon 2017 (see *http://iocs.ioccg.org/programme/conference-materials/)*

Richard Gilmore ***Introduction to Copernicus Program*** *(Sentinel and CMEMS)*

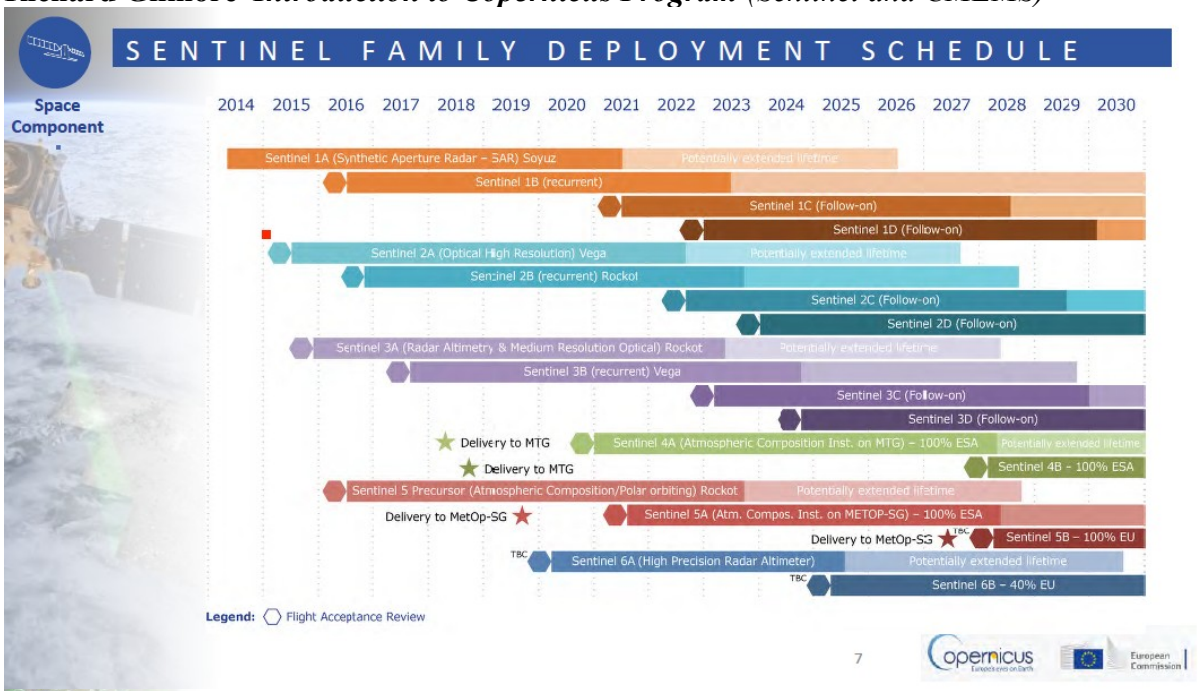

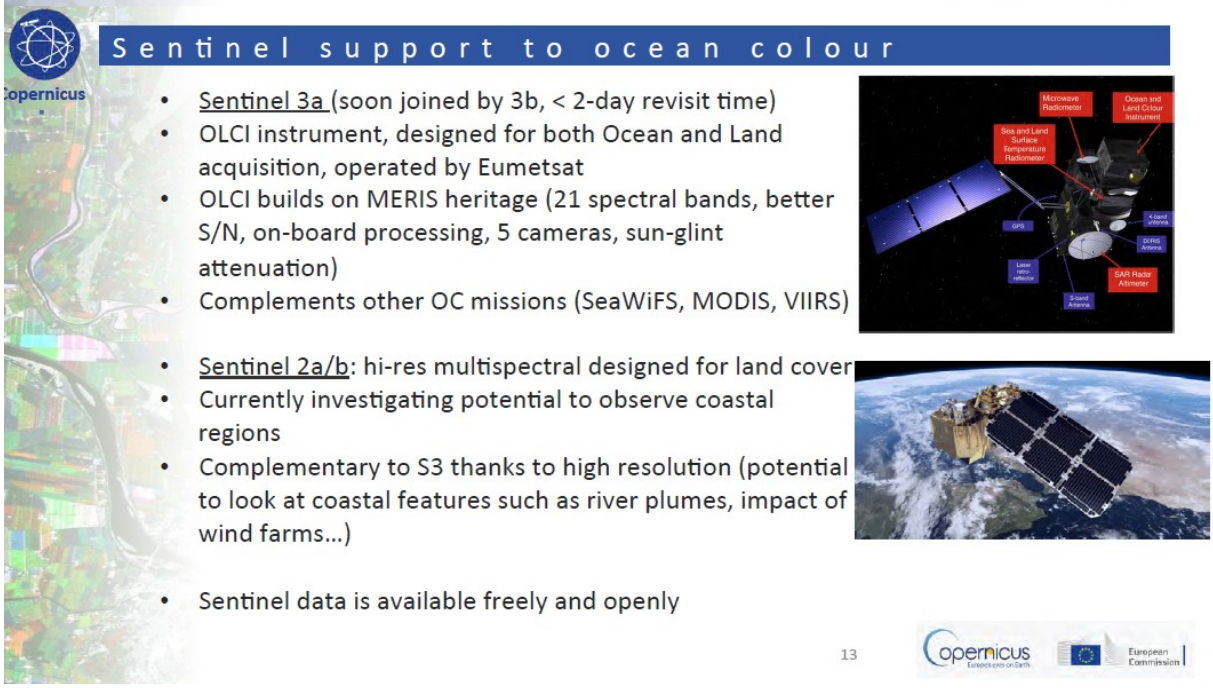

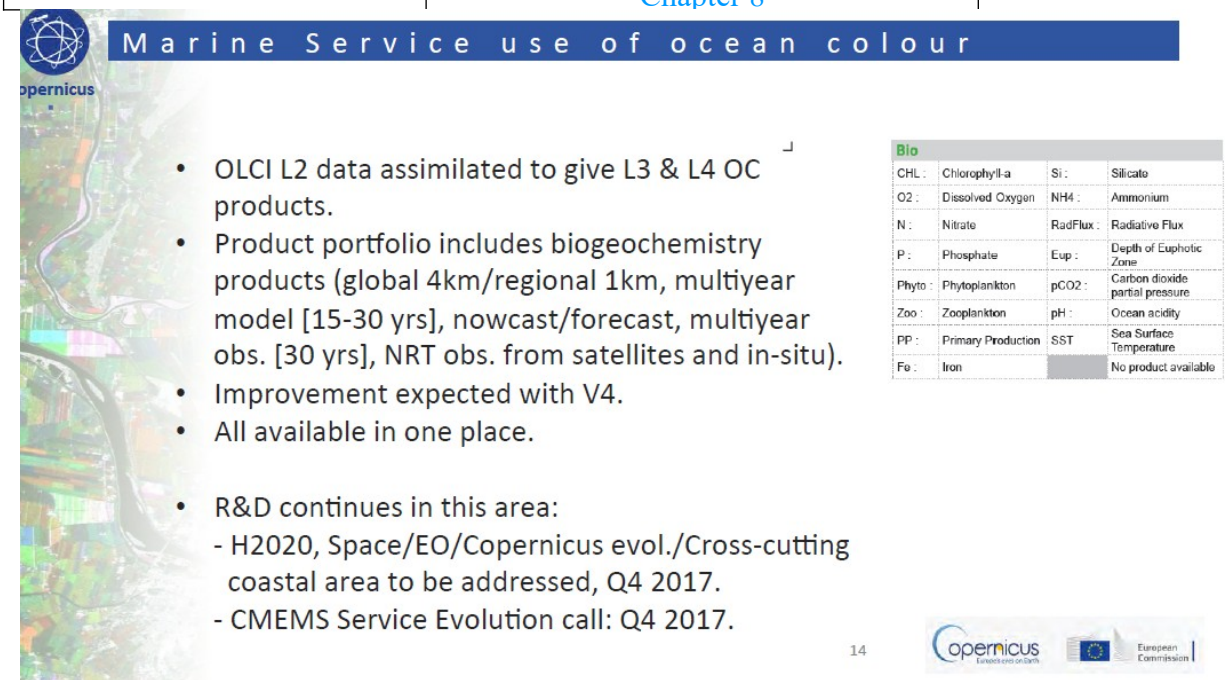

Anne Lifermann *"CNES support to ocean colour science"*

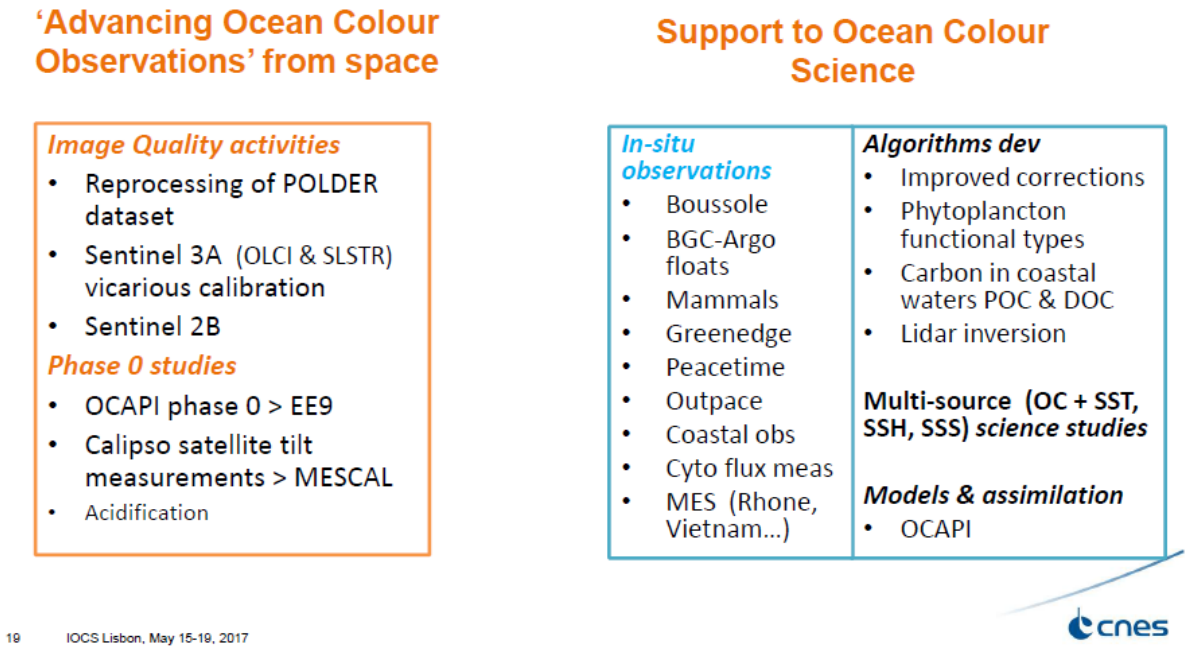

International activities:

09:15 – 09:30 *Korean geostationary ocean colour missions, GOCI and GOCI-II (Seongick Cho)*

- **09:30 – 09:45** CONAE: Missions and initiatives for coasts and oceans (Sandra Torrusio)
- **09:45 – 10:00** ISRO: Ocean colour activities in India (Prakash Chauhan)
- **10:00 – 10:15** Update on Chinese ocean colour satellite missions (Zhihua Mao)

Bryan Franz ***NASA OBPG/satellite ocean colour update***

NASA Ocean Biology Processing Group

currently supporting calibration, validation, software development, (re)processing, and distribution for a multitude of ocean color missions & sensors.

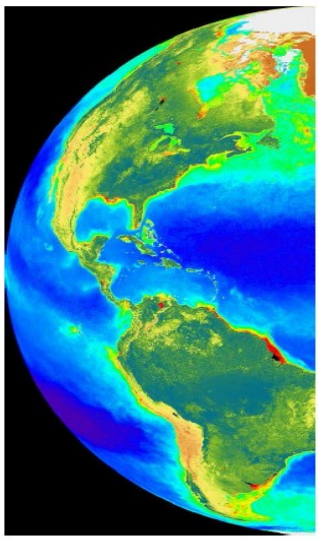

Global Processing & Distribution

- **VIIRS/NPP** (USA)
- **MODIS/Aqua** (USA)
- **MODIS/Terra** (USA)
- **OLCI/S3A** (Europe)
- SeaWiFS (USA)
- CZCS (USA)
- MERIS (Europe)
- OCTS (Japan)

Regional Processing & Distribution

- **GOCI** (Korea)
- HICO (USA)

Limited Mission Support

- Landsat-8/OLI (USA)
- Sentinel-2/MSI (Europe)
- OCM-1/2 (India)
- OSMI (Korea)
- MOS (Germany/India)

Ocean Color Reprocessing

All global missions are now at version R2014.0 (with the exception of MERIS).

Reprocessing R2014.0 included:

- updates to instrument and vicarious calibrations
- updates to standard algorithms (e.g., OCI Chlorophyll)
- expansion of standard products to include suite of inherent optical properties (GIOP).
- switch to NetCDF4 file formats (Level-2 and Level-3)

We have **not** reprocessed any ocean color missions in the past year!

Rrs(λ) Validation

all available in situ match-ups from SeaBASS & AERONET-OC

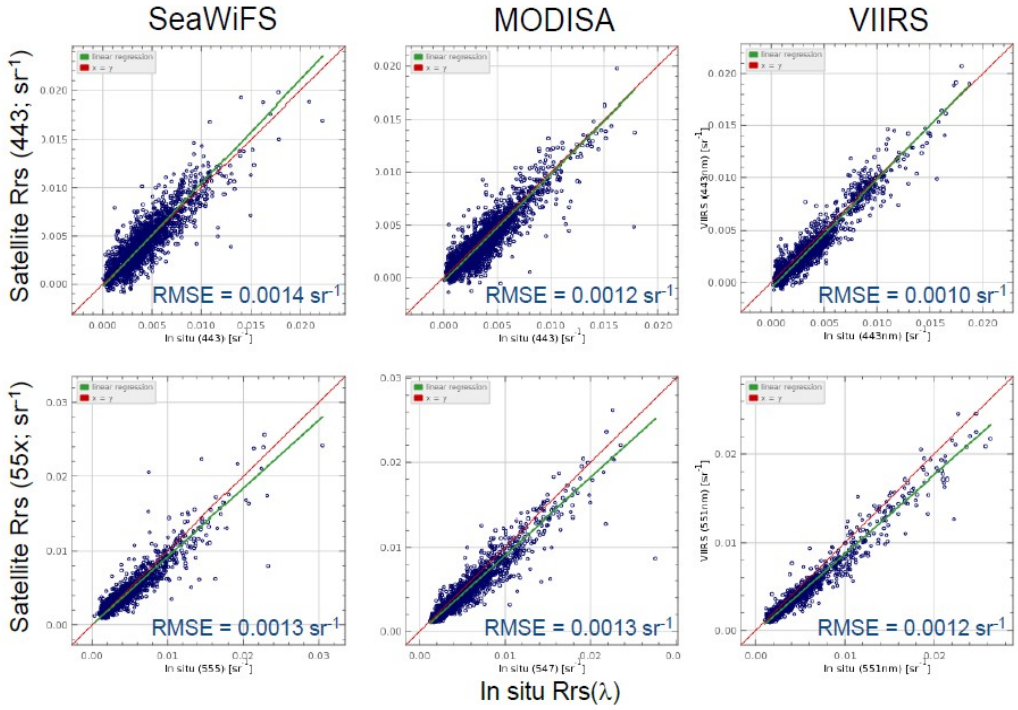

Chlorophyll-a Validation

all available in situ match-ups from SeaBASS

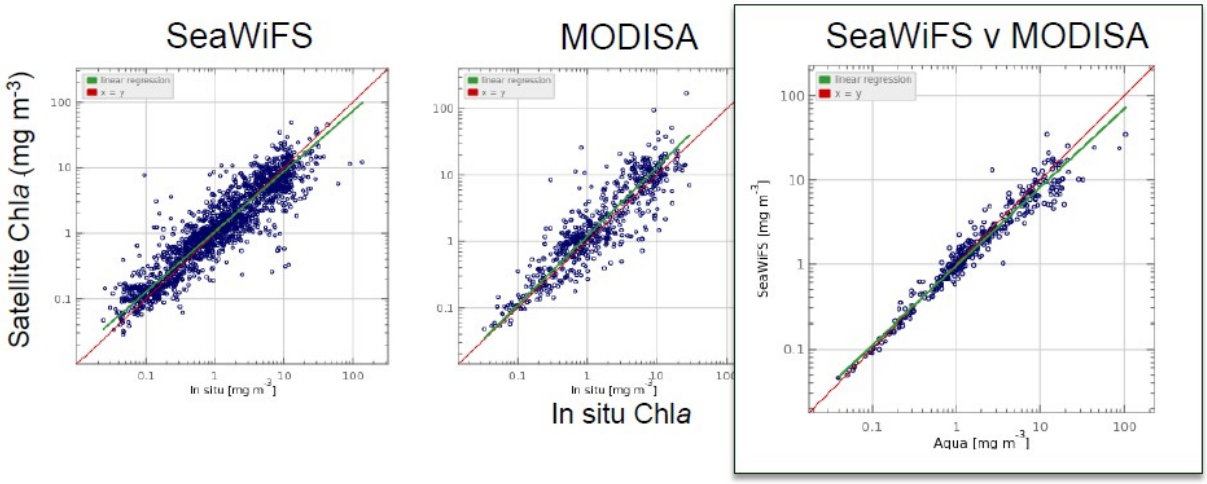

in VIIRS era

- heavy reliance on AERONET-OC for radiometric validation
- need more 2012-2017 chlorophyll in SeaBASS!

Long-term (19-year) Chlorophyll Record

multiple missions, consistently processed

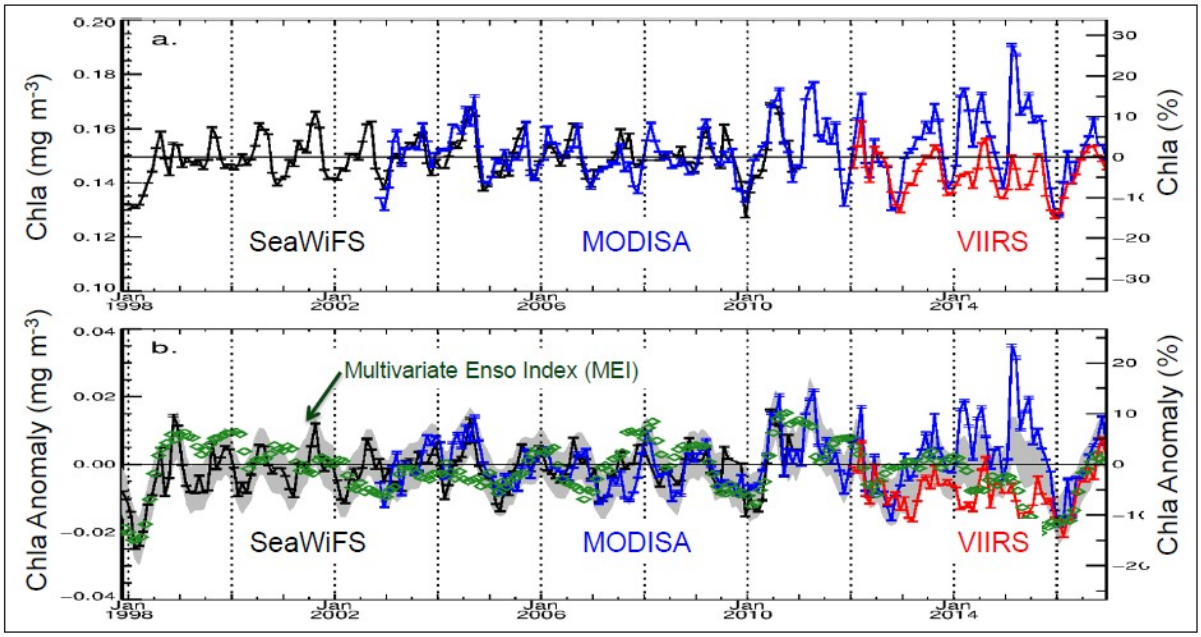

known issues with MODIS/Aqua data quality after 2012

OLCI Processed with SeaDAS

using standard NASA algorithms

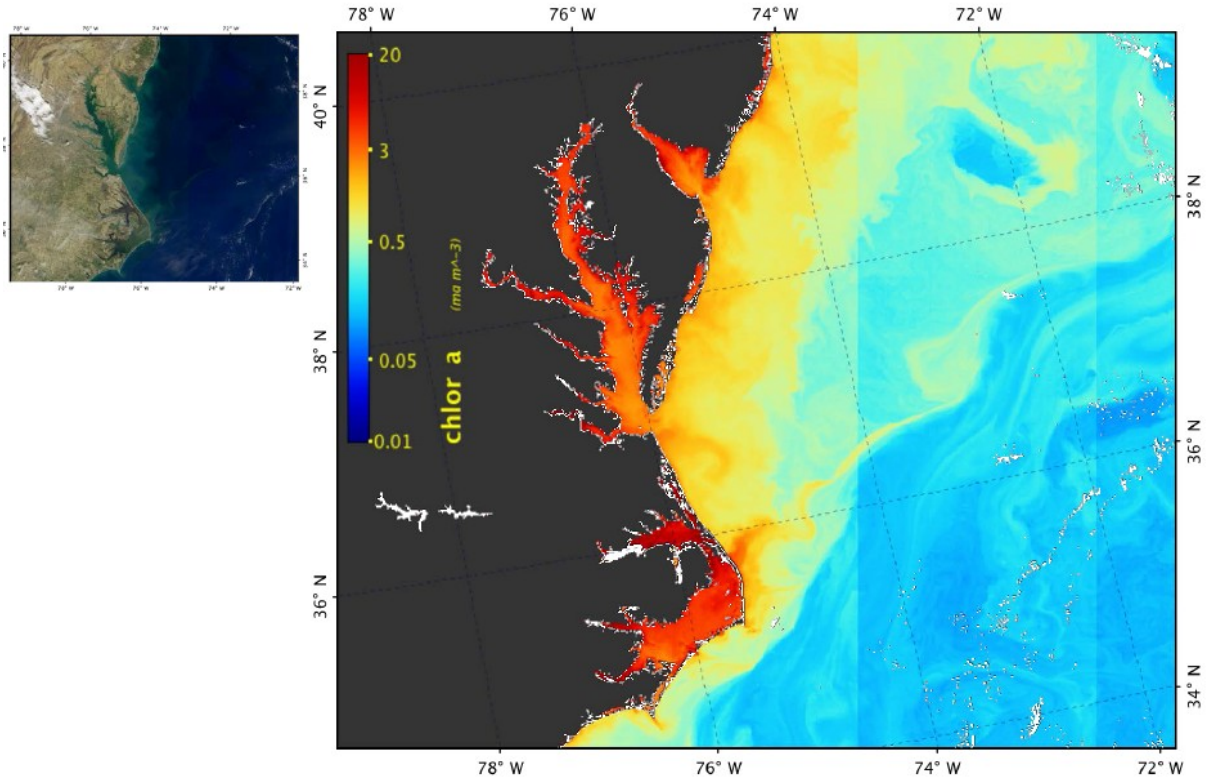

Chlorophyll-a Comparison of VIIRS and OLCI

using standard NASA algorithms

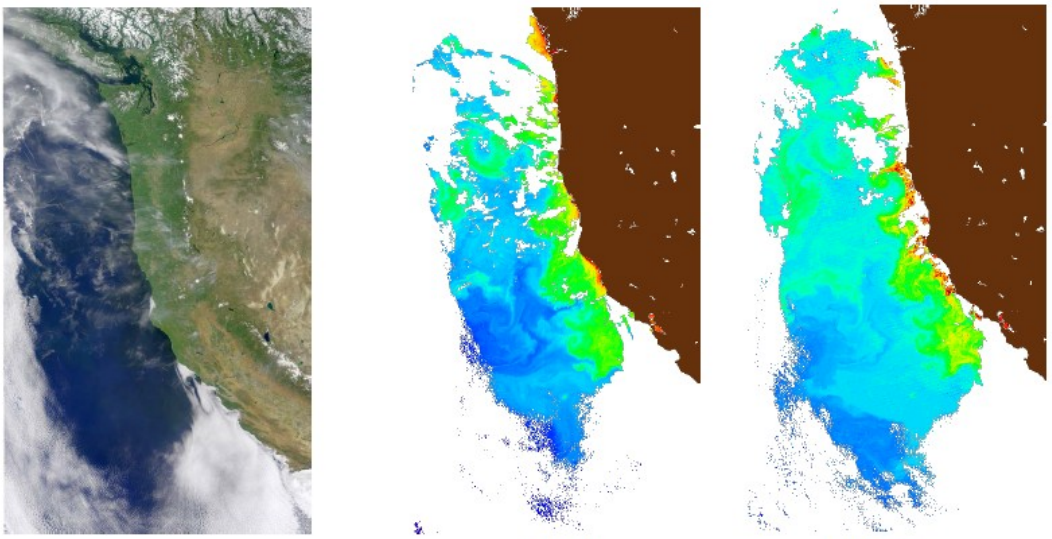

Sentinel-3 OLCI Support (ESA)

- Processing capability
  - standard NASA ocean color processing codes have been augmented to support OLCI
  - processing capability from Level-1B with NASA algorithms is supported in current SeaDAS
  - refinements to incorporate updated spectral response and implement smile correction in progress
- Data distribution
  - OBPG is acquiring full OLCI mission at Level-1B, through ESA-NASA gateway (FR/RR, archived from start of commissioning)
  - distribution (mirror) of RR Level-1B via ocean color web portal, with FR coming soon
  - **anticipating full mission Level-1B update from ESA**
  - production & distribution of NASA Level-2 is TBD

HISTORICAL OVERVIEW OF "OCEANOGRAPHIC" SATELLITE MISSIONS

Seasat June 27, 1978 after 99 days central system failure;
800 km close polar orbit; covering 95% of the earth's surface; SAR 25 m resolution

Nimbus 7 Oct 78 -> mid-1986
COASTAL ZONE COLOR SCANNER

CZCS:	**443, 520, 550, 670 (20 nm)**	**ocean colour**
	700 – 800 nm	surface vegetation
	10,500 – 12,500 nm	surface T

SPOT (**Système Probatoire d'Observation de la Terre** or **Satellite Pour l'Observation de la Terre**) is a family of French Earth observation satellites developed by the French space agency, CNES (Centre national d'études spatiales). The first five were launched between 1985 and 2002. The images supplied by the satellites are sold through Astrium. Spot 6 was launched in 2012 and SPOT 7 is expected for 2014.

- Resolution of produced images:
  - Panchromatic: 1.5 m (b/w)
  - Colour: 1.5 m
  - Multispectral: 6 m
- Spectral bands, simultaneous panchromatic and multispectral acquisition in the following bands:
  - Panchromatic (455 – 745 µm)
  - Blue band (455 – 525 µm)
  - Green band (530 – 590 µm)
  - Red band (625 – 695 µm)
  - NIR band (760 – 890 µm)
- Swath: 60 km by 60km
- Reactive programming: 6 programming plans per day for each satellite
- Acquisition capacity: 3 million km² per day
- Launch dates: SPOT 6 was launched on 9 September 2012 by an Indian PSLV

SeaStar satellite **from September 1997** (11y after CZCS) **till 2010**

SeaWiFS: Sea-Viewing Wide Field-of-View Sensor

low Earth, circular, parking orbit at an altitude of 278 km with an inclination of 98° 20'; solar panels with batteries

Band	Center Wavelength (nm)	Bandwidth
1	412	20
2	443	20
3	490	20
4	510	20
5	555	20
6	670	20
7	765	40
8	865	40

LAC data (1.1 km at nadir); GAC (4.4 km at nadir)
three levels of processing

MODerate resolution Imaging Spectrometer (MODIS)
36 wavelengths
NASA Earth Observing System (EOS)
in 1999 aboard the Terra satellite (EOS AM – descending orbit),
in 2002 aboard the Aqua (EOS PM – ascending orbit)

Band/wavelength/resolution

8	405–420	1000m	
9	438–448	1000m	
10	483–493	1000m	
11	526–536	1000m	Ocean Color/
12	546–556	1000m	Phytoplankton/
13	662–672	1000m	Biogeochemistry
14	673–683	1000m	
15	743–753	1000m	
16	862–877	1000m	

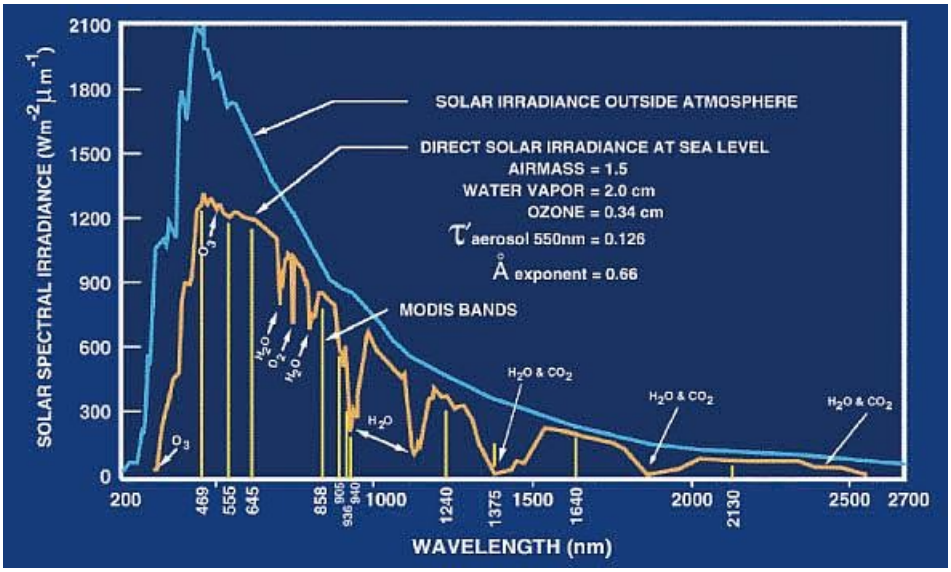

MODIS_ATM_solar_irradiance.jpg

ENVISAT May 2000 5y ESA polar
MEdium Resolution Imaging Spectrometer (MERIS) 1150 km
Spectral range: 390 nm to 1040 nm (sun no clouds)
Spectral resolution: 2.5 nm
Band transmission capability:
Up to 15 spectral bands, programmable in position and width
ASAR (5.3 GHz; C band) active SAR reflectivity (irrespective of cloud cover)
DORIS (Doppler Orbitography and Radiopositioning Integrated by Satellite)
ozone monitoring, stratosphere chemistry
http://envisat.estec.esa.nl/

ADEOS II launched in 2000 (Japanese satellite)
ADEOS until 97
Ocean Color and Temperature Scanner (OCTS) 12 bands visible + IR
Polarization and Directionality of the Earth's Reflectance (POLDER) CNES
angular characteristics of the earth's reflectance (14 directions)
scanned four times every 5 days
NASA Scatterometer (NSCAT)
active microwave radar to measure wind speed and direction over the oceans
by transmitting Ku band microwave pulse (13.995 GHz; 0.75cm to ~2.5cm)

OCM Ocean Color Monitor (India) satellite: IRS – P4 (since 99)
wavelengths: 414, 442, 489, 512, 557, 670 nm (resolution 20 nm)
and 768 and 867 nm (resolution 40 nm)
every two days

Gaofen (= "high resolution") is a family of Chinese high-resolution earth observation satellites for the Chinese state-sponsored programme called "High-resolution Earth Observation System" (CHEOS). The first Gaofen satellite, Gaofen 1, was launched in 2013.

Big change with the advent of SpaceX which recycles the rockets and will put more scientific sensors into orbit (e.g., SWOT in 2021).

Supplement: From https://fr.wikipedia.org/wiki/Elon_Musk

Elon Reeve Musk (1971, Pretoria) is an entrepreneur, business manager and engineer of South African origin, naturalized Canadian in 1988 and then American in 2002. He is currently based in Los Angeles. He is the CEO and CTO of SpaceX Company as well as CEO, Director of Product Architecture of Tesla Company, and former Chairman of the Board of SolarCity and Tesla. He is also the founder of The Boring Company, a tunnel construction company, and Neuralink, a neurotechnology company.

In June 2002, disillusioned by NASA, which he considered lacking in ambition, Elon Musk founded his third company, Space Exploration Technologies (SpaceX), of which he is the current CEO and CTO. SpaceX develops and produces reusable first-stage space launch vehicles (eventually, same day), with the goal of lowering launch costs and, in the long term, making the colonization of Mars possible. SpaceX developed the Falcon 1 and Falcon 9 rockets as well as the Dragon cargo ship.

From 2012, SpaceX refuelled the International Space Station.

By the end of 2013, he aims to create a supersonic electric plane that could take off and land vertically, as well as to found a colony of a million people on Mars.

In December 2015, Space X carried out the first recovery of the first stage of its Falcon 9 rocket.

In March 2017, SpaceX's first "recycled" Falcon 9 was launched, using a first stage that had already flown in April 2016.

On February 6, 2018 Space X launches the first Falcon Heavy, with Elon Musk's red Tesla Roadster on board. The launch is successful and Space X recovers the 2 secondary thrusters but does not recover the middle stage. This marketing stunt puts Space X and Tesla into 'orbit' on social media and television around the world.

On November 16, 2020, the Falcon 9 launcher is used to send a crew of 4 astronauts (compared to 3 with Soyuz launches) to the international space station.

Hyperspectral
NASA PACE ocean colour sensor
expected launch in 2022
https://pace.gsfc.nasa.gov/
Sensor: Ocean Color Instrument (OCI)
Field of view:
0.08° along track and 1.42° cross track.
Coverage:
2-day global coverage at 1-km (0.6-mi) resolution.
Spectral coverage:
Hyperspectral radiometry from the **ultraviolet (350 nm) to near-infrared (885 nm).**
Grating that splits the incoming light into **5nm increments**
see: https://pace.oceansciences.org/events_more.htm?id=9
+ SWIR bands:
Shortwave (SW) infrared (IR) bands include:
940, 1038, 1250, 1378, 1615, 2130, and 2260 nm.
Calibration:
Total calibration of instrument artefacts <0.5% at top-of-atmosphere.

The OCI will feature:

- Cross track, 360° continuous rotating telescope
- Two slit grating hyperspectral spectrographs (ultraviolet to visible & visible to near-infrared, NIR)
- Fiber-coupled multiband filter spectrograph (NIR-to shortwave-infrared)

See slide 45 of the presentation by J. Uitz
What is the advantage of going hyperspectral?

Ability to use certain inflection points of the curves (detected, for example, by taking the 2nd or 4th derivative)
Is there really an advantage compared to spectral? See Roesler 2004
It seems like we may not need to switch to hyperspectral for open ocean observations since the Chl concentration is low and there exists a mix of species.

Hammann et Puschell, SeaWiFS-2: an ocean color data continuity mission to address climate change, Remote Sensing System Engineering II, edited by Philip E. Ardanuy, Jeffery J. Puschell, Proc. of SPIE Vol. 7458, 745804 · © 2009 SPIE

Current Ocean-Colour Sensors (http://www.ioccg.org/sensors/current.html) early 2016

SENSOR	AGENCY	SATELLITE	LAUNCH DATE	SWATH (km)	SPATIAL RESOLUTION (m)	BANDS	SPECTRAL COVERAGE (nm)	ORBIT
COCTS CZI	CNSA (China)	HY-1B (China)	11 April 2007	2400 500	1100 250	10 4	402 - 12,500 433 - 695	Polar
GOCI	KARI/ KORDI (South Korea)	COMS	26 June 2010	2500	500	8	400 - 865	Geostationary
HICO	ONR and DOD Space Test Programme	JEM-EF Int. Space Stn.	18 Sept. 2009	50 km Selected coastal scenes	100	124	380 - 1000	51.6°, 15.8 orbits p/d
MERSI	CNSA (China)	FY-3A (China)	27 May 2008	2400	250/1000	20	402-2155	Polar
MERSI	CNSA (China)	FY-3B (China)	5 November 2010	2400	250/1000	20	402-2155	Polar
MODIS-Aqua	NASA (USA)	Aqua (EOS-PM1)	4 May 2002	2330	250/500/1000	36	405-14,385	Polar
MODIS-Terra	NASA (USA)	Terra (EOS-AM1)	18 Dec. 1999	2330	250/500/1000	36	405-14,385	Polar
OCM-2	ISRO (India)	Oceansat-2 (India)	23 Sept. 2009	1420	360/4000	8	400 - 900	Polar
POLDER-3	CNES (France)	Parasol	18 Dec. 2004	2100	6000	9	443-1020	Polar
VIIRS	NOAA /NASA (USA)	NPP	28 Oct. 2011	3000	370 / 740	22	402 - 11,800	Polar

For May 2016, the table only contains: COCTS, GOCI,MODIS aqua and Terra, OCM2, OLCI and VIIRS with

OLCI	ESA/ EUMETSAT	Sentinel 3A	16/02/16	1270	300/1200	21	400 - 1020	Polar

https://sentinel.esa.int/web/sentinel/technical-guides/sentinel-3-olci/olci-instrument/spectral-response-function-data

Main hyperspectral sensors on aircraft and satellites Table 1

Hyperspectral sensors on satellites			
Types of sensors	**Producer**	**Number of bands**	**Spectral range [µm]**
FTHSI on MightySat II	Air Force Research	256	0.35-1.05
Hyperion on EO-1	NASA Guddard Space Flight Center	242	0.40-2.50
Hyperspectral sensors on aircrafts			
AVIRIS (Airborne Visible Infrared Imaging Spectrometer)	NASA Jet Propulsion Lab.	224	0.40-2.50
HYDICE (Hyperspectral Digital Imagery Collection Experiment)	Naval Research Lab.	210	0.40-2.50
PROBE-1	Earth Search Sciences Inc.	128	0.40-2.50
CASI (Compact Airborne Spectrographic Imager)	ITRES Research Limited	Over 228	0.40-1.00
HyMap	Integrated Spectronics	100 la 200	Visible to termal infrared
EPS-H (Environmental Protection System)	GER Corporation	VIS/NIR (76), SWIR1 (32), SWIR2 (32), TIR (12)	VIS/NIR (0.43-1.05) SWIR1 (1.50-1.80) SWIR2 (2.00-2.50) TIR (8-12.50)
DAIS 7915 (Digital Airborne Imaging Spectrometer)	GER Corporation (Geophysical and Environmental Research Imaging Spectrometer)	VIS/NIR (32), SWIR1 (8), SWIR2 (32), MIR (1), TIR (12)	VIS/NIR (0.43-1.05) SWIR1 (1.50-1.80) SWIR2 (2.00-2.50) MIR (3.00-5.00) TIR (8.70-12.30)
DAIS 21115 (Digital Airborne Imaging Spectrometer)	GER Corporation	VIS/NIR (76), SWIR1 (64), SWIR2 (64), MIR (1), TIR (6)	VIS/NIR (0.40-1.00) SWIR1 (1.00-1.80) SWIR2 (2.00-2.50) MIR (3.00-5.00) TIR (8.00-12.00)
AISA (Airborne Imaging Spectrometer)	Spectral Imaging	Over 288	0.43-1.00

Vorovencii, Bulletin of the *Transilvania* University of Brasov • Vol. 2 (51) - 2009 • Series II

Hyperspectral sensors are characterized by the fact that they produce records in a large number of adjacent and narrow lanes thereby providing a very high spectral resolution. In this way, interpretations and analyses can be made of the remote images at the micro-level, highlighting the features of details which could not be underlined with multispectral sensors

ACCESS TO DATA/INTERNET ADDRESSES

Image types available now or in the future

•Images of sun-synchronous sensors to measure ocean colour (MERIS/MODIS/VIIRS/OLCI)
•Images of high spatial resolution (SPOT, Pleiades, Landsat, Sentinel2)
•Hyperspectral aerial or satellite images (CASI/HySpex/HICO)
•Images from geostationary satellites (Meteosat/GOCI/OCAPI)

FREE:

SST NOAA/AVHRR

http://poet.jpl.nasa.gov/
http://www.cdc.noaa.gov/map/
http://coralreefwatch.noaa.gov/satellite/archive/archive_chart_sst50km_2006.html
(twice weekly composite)

Suggestions for site where you can see ocean colour images

MODIS (world view)
https://worldview.earthdata.nasa.gov/?p=geographic&l=VIIRS_SNPP_CorrectedReflectance_TrueColor(hidden),MODIS_Aqua_CorrectedReflectance_TrueColor(hidden),MODIS_Terra_CorrectedReflectance_TrueColor,MODIS_Aqua_Chlorophyll_A,MODIS_Terra_Chlorophyll_A,Reference_Labels(hidden),Reference_Features(hidden),Coastlines&t=2017-07-28&z=3&v=-74.86981355042028,-11.600676207983168,-22.205751050420282,13.500886292016832&ab=off&as=2017-09-18&ae=2017-09-25&av=3&al=false

https://worldview.earthdata.nasa.gov/

MODIS and VIIRS – SST, chla, AFAI (Hu), etc – certain geographical zones
http://optics.marine.usf.edu/cgi-bin/optics_data?roi=C_ATLANTIC&current=1

Ocean color site to download data from MODIS, VIIRS, etc... + daily/monthly composites, etc
https://oceancolor.gsfc.nasa.gov/cms/#

Visualisation + download – high resolution satellite (Landsat- Sentinel; with terrestrial applications)
https://earthexplorer.usgs.gov/

Same for Europe.
https://scihub.copernicus.eu/

With on-line catalogue:

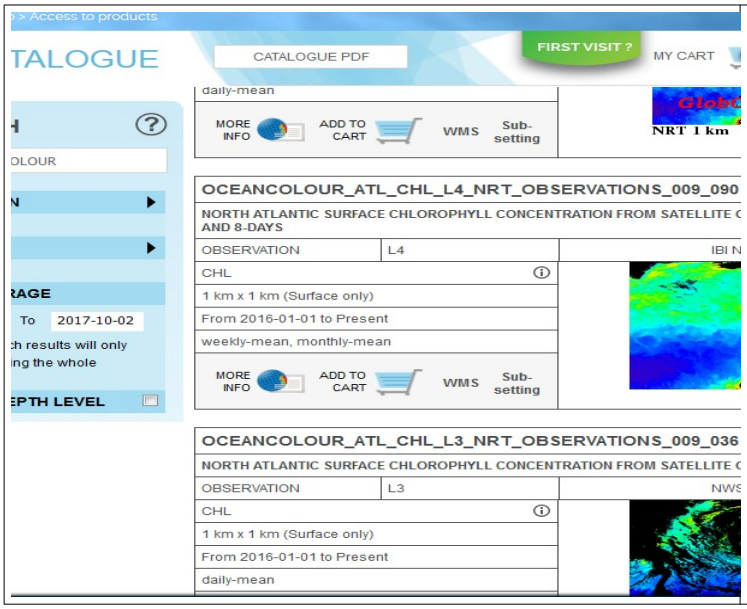

http://marine.copernicus.eu/services-portfolio/access-to-products/

Your search : OCEANCOLOUR
select as parameter:
plankton

Make sure that the 3rd line contains "observation" and not "model"

Visualisation of certain data (to be tested; essentially made for Mars but can be applied to Earth as well) https://jmars.asu.edu/

OC view (NOAA)
https://www.star.nesdis.noaa.gov/sod/mecb/color/VIIRS_EDR_Composite.php

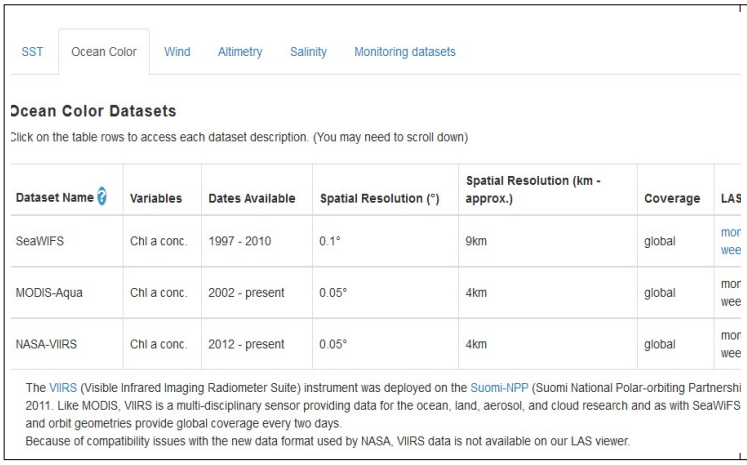

http://oceanwatch.pifsc.noaa.gov/doc.html#chl

with data accessible via ERRDAP

ESA: http://www.globcolour.info/data_access.html

The Full Product Set (FPS), also called GLOB_4KM, covers the merged Level-3 ocean color products in the time period 1997-today.

The FPS data set consists of ocean color merged data products using the merging algorithms recommended at the first GlobColour workshop in Villefranche sur mer (France) on the 4-6 December 2006. The FPS includes level 3 merged products as daily, 8-days and monthly averaged products mapped on a common ISIN 4.63km grid.

FPS archive products (RAN, at D+30) are available on a dedicated ftp server or though the HERMES data portal (see below). Global products at 4.6 km resolution are available (GLOB_4KM) as well as several specific large regions of interest at different spatial resolutions (EURO_4KM, EURO_2KM, ...)

A full scale validation has been performed and all results have been presented at the second user workshop, in Oslo, on November 20-22 2007.

Distributed merged products are:

Chlorophyll-a, case I water (CHL1),
Chlorophyll-a, case II water (CHL2),
Total Suspended Matter (TSM),
Coloured dissolved and detrital organic materials (CDM),
Particulate back-scattering coefficient (bbp),
Diffuse attenuation coefficient (KD490),
Fully normalised water-leaving radiances at 412, 443, 490, 510, 531, 550-565, 620, 665-670, 681 and 709 nm (Lxxx),
Relative excess of radiance at 555 nm (EL555),
Aerosol optical thickness over water (T865),
Cloud Fraction (CF).

NASA: http://oceancolor.gsfc.nasa.gov/

Altimetry/Currents – TOPEX, JASON

http://www-ccar.colorado.edu/~realtime/global_realtime/geovel.html
Map of geostrophic currents derived from altimetry data (latitudes from 66 S to 37 N; does not include the Gulf of Lion; default values give the Gulf of Mexico)

http://www.jason.oceanobs.com/ in French
http://www.aviso.oceanobs.com/fr/kiosque/les-plus-belles-images-de-l-altimetrie-autour-du-monde/index.html
The most beautiful images of altimetry applications under Google Earth: currents, eddies, geoid, bathymetry, ...

PAID or SUBSCRIPTION

Visible - SPOT

SPOT IMAGE (F): http://www.spot.com/ since 1986
Resolution 2.5 m instead of 10 m; HSR mode (High Stereoscopic Resolution: 3D reconstruction of the earth's relief "digital terrain models"

SAR - ERS1-ERS2

ESA: http://earth.esa.int/object/index.cfm?fobjectid=4001

LANDSAT
EURIMAGE: http://www.eurimage.com/
Landsat 7 data is not available for acquisitions after 31 May 2003, due to mechanical problems with the ETM+ sensor

wind and altimetry
CERSAT (F): http://www.ifremer.fr/cersat/

EUMETSAT: http://www.eumetsat.de/en/
joint European/US polar satellite system. EUMETSAT plans to assume responsibility for the "morning" (local time) orbit and the US will continue with the "afternoon" coverage. EUMETSAT instruments are now on the METOP satellite, developed in cooperation with ESA.

e.g., Satellite Receiving stations:

METEO-FRANCE at TOULOUSE

ACRI (Sophia-Antipolis, France): http://www.acri.fr/French/esa.html
MERIS

Dundee (UK): http://www.sat.dundee.ac.uk/
AVHRR, SeaWiFS, Seviri, MODIS
Or other site: http://www.neodaas.ac.uk/

(NEODAAS = Natural Environment Observation Data Acquisition and Analysis Service)

DLR/ISIS (D): http://isis.dlr.de/

Applications
http://envisat.esa.int/live/
Assimilated Ozone Field (North Pole)
Cloud structures with MERIS data
Near-real-time Sea Level Anomalies
Mercator Ocean maps: Global Ocean Surface Temperature
MERIS Level 1 "Image of the Day"
MERIS Global Coverage Quicklooks

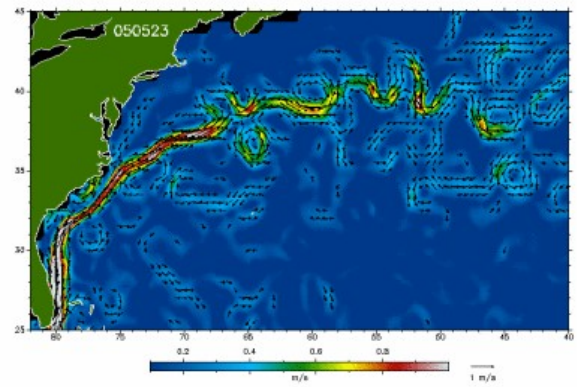

This image shows the variation of the Gulf Stream velocities near the East coast of North America in the last 20 days. The images are updated daily and the velocities are in metres per second (to get the approximate velocity in knots, multiply by 1.9438445).

Since 22 July 2003 the Gulf Stream velocity fields derive from near-real-time radar altimeter data of the European Environmental Satellite Envisat. At the same time the mapped area was increased to show more upstream regions of the Gulf Stream.

Source: DEOS (Department of Earth Observation and Space Systems, Delft University).

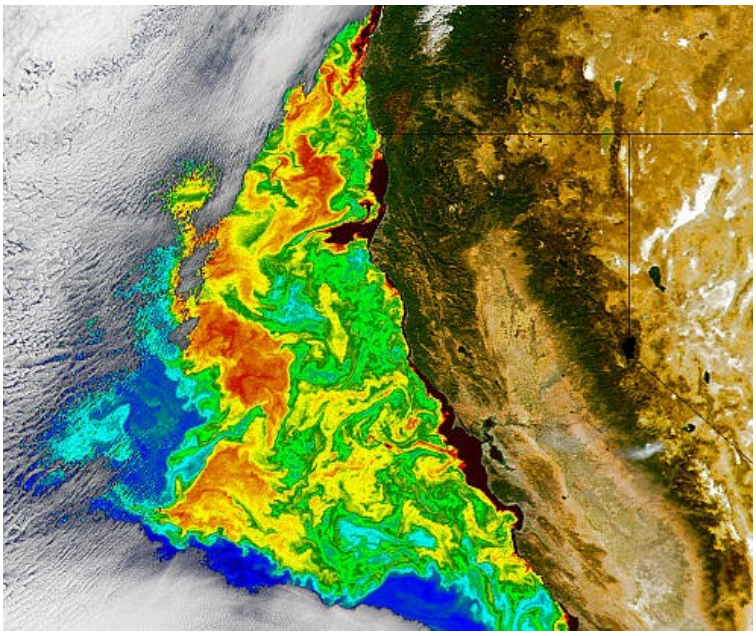

http://oceancolor.gsfc.nasa.gov/cgi/image_archive.cgi?c=COASTAL

SeaWiFs image of (6 October 2002) chlorophyll concentration; clouds and earth are represented in near-natural colours.

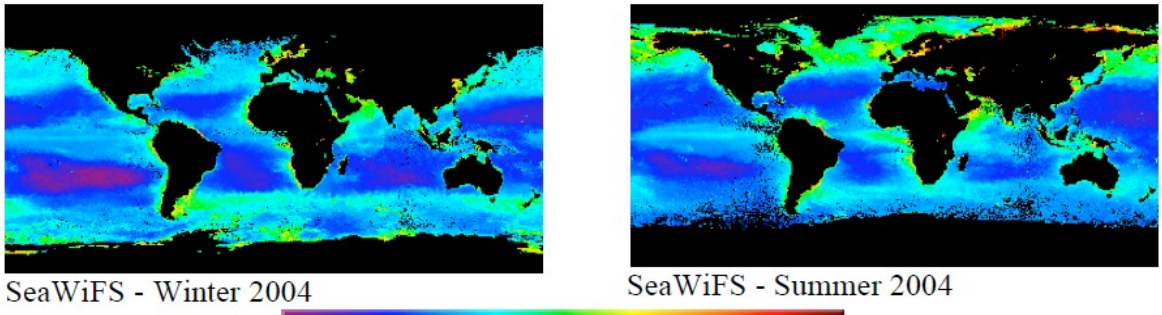

UV measurements

At present there are only two sensors capable of detecting UV:
1) DAIS (IRD) which is currently equipped on an aircraft.
2) FTHSI on the MightySat 2 satellite belonging to the US Air Force.
There are currently proposals being made to launch a SeaWifs-2 which would be able to detect UV; in order to reduce the launch cost a small launcher such as Pegasus would be used.

Note: International Space Station (ISS), in orbit since 20 Nov 98 (altitude ~350 km)
http://earthobservatory.nasa.gov/Newsroom/NewImages/images.php3?img_id=17413

Below an some example SAR images

ISS013-E-71473

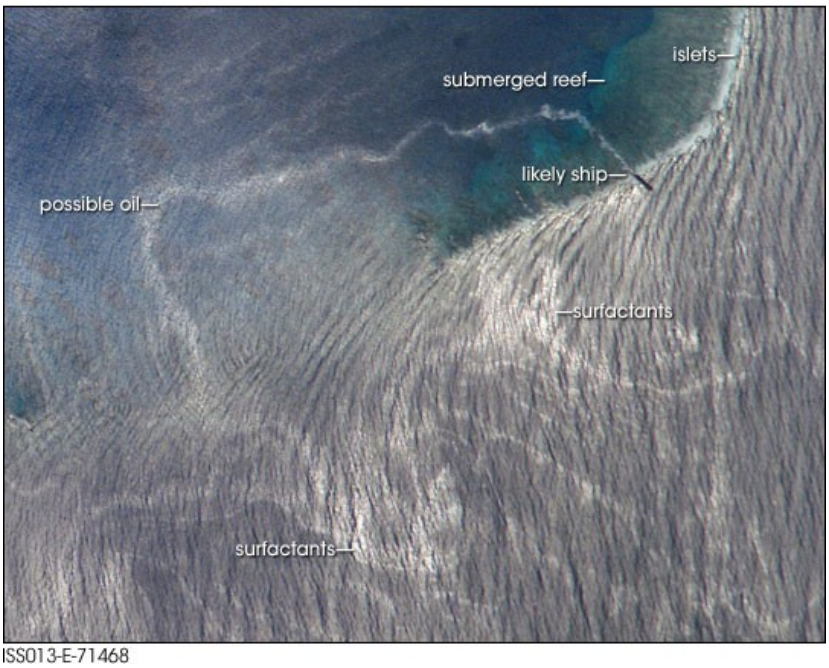

ISS013-E-71468

Photos of surface swell near Bajo Nuevo Reef, Caribbean Sea
27 August 2006